



**HAL**  
open science

# Ultrafast Laser Volume Nanostructuring of Transparent Materials: From Nanophotonics to Nanomechanics

Razvan Stoian, Ciro D'amico, Yves Bellouard, Guanghua Cheng

► **To cite this version:**

Razvan Stoian, Ciro D'amico, Yves Bellouard, Guanghua Cheng. Ultrafast Laser Volume Nanostructuring of Transparent Materials: From Nanophotonics to Nanomechanics. Ultrafast Laser Nanostructuring, 239, Springer International Publishing, pp.1053-1084, 2023, Springer Series in Optical Sciences, 10.1007/978-3-031-14752-4\_29 . ujm-04082764

**HAL Id: ujm-04082764**

**<https://ujm.hal.science/ujm-04082764>**

Submitted on 14 Oct 2023

**HAL** is a multi-disciplinary open access archive for the deposit and dissemination of scientific research documents, whether they are published or not. The documents may come from teaching and research institutions in France or abroad, or from public or private research centers.

L'archive ouverte pluridisciplinaire **HAL**, est destinée au dépôt et à la diffusion de documents scientifiques de niveau recherche, publiés ou non, émanant des établissements d'enseignement et de recherche français ou étrangers, des laboratoires publics ou privés.

# Ultrafast laser volume nanostructuring of transparent materials; from nanophotonics to nanomechanics

Razvan Stoian, Ciro D'Amico, Yves Bellouard, and Guanghua Cheng

**Abstract** The capability of ultrashort laser pulses to generate nonlinear absorption in the transparency window of dielectric materials is at the base of volume structuring. The result is a local change of the refractive index, the building block for generating complex embedded optical functions in three-dimensional geometries within a monolith chip. The nonlinearity determines spatial scales on the order of the wavelength. Depending on the rate and the amount of energy deposition, the local refractive index change can be accurately tuned from positive to negative values on variable scales, generating thus new capabilities for processing light within an optical chip in terms of embedded waveguides and micro-optics. New irradiation strategies and engineered glasses permit to go even further in reaching processing super-resolution, i.e. on spatial scales smaller than the optical resolution. The smallest scales achievable nowadays go well below the diffraction limit approaching and even surpassing the 100 nm value, a tenth of the wavelength. We will discuss in this chapter the possibility of obtaining structural features much smaller than the electromagnetic wavelength and the associated methods. Direct focusing and self-organization phenomena will be analyzed, as well as the optical functions originating from these processes, namely in transporting and manipulating light. Achieving extreme scales in the range of 100 nm generates an additional capability

---

Razvan Stoian (corresponding author)

Laboratoire Hubert Curien, UMR 5516 CNRS, Université Jean Monnet, 42000 Saint Etienne, France, e-mail: razvan.stoian@univ-etienne.fr

Ciro D'Amico

Laboratoire Hubert Curien, UMR 5516 CNRS, Université Jean Monnet, 42000 Saint Etienne, France, e-mail: ciro.damico@univ-st-etienne.fr

Yves Bellouard

Galatea Lab, STI/IEM, Ecole Polytechnique Fédérale de Lausanne (EPFL), 2002 Neuchâtel, Switzerland, e-mail: yves.bellouard@epfl.ch

Guanghua Cheng

School of Electronics and Information, Northwestern Polytechnical University, 710072 Xi'an, Shaanxi, China, e-mail: guanghuacheng@nwpu.edu.cn

to sample the electrical field within the optical chip and thus to process and read-out optical signals. We will discuss emerging applications ranging from photonics, such as sensors, spectro-imagers, actuators or supports for data storage, down to nanomechanical systems, and pinpoint the enabling character of extreme nanostructuring scales using ultrafast lasers.

**Key words:** Laser Volume Nanostructuring, Optical Resolution, 3D Photonics, Integrated Optical Circuits, Sampling Electrical Fields.

## 1 Introduction

Laser volume structuring of transparent materials is based on a straightforward irradiation concept. This concept implies first a capability to transport energy to the point of impact (focus location) without losses and, secondly, to deposit the energy from the beam to the material in a restricted spatial domain around the point of impact. In most of the cases it implies the crossing of a dielectric interface and the focusing inside the volume of the material. A perfectly adapted tool for this task is an ultrashort laser pulse. Typically generated at wavelengths for which the material is intrinsically transparent (mostly in the near-infrared and in the visible range), the propagating ultrashort laser pulse increases its intensity upon focusing up to the point where a nonlinear absorption process is triggered within the confocal volume. This nonlinear excitation process sustained by high intensities occurs as a combination of multiphoton, field, and collisional ionization events. For intensities in the TW/cm<sup>2</sup> range free charge carriers are generated across the material forbidden bandgap at densities that approach the material molecular density (10<sup>22</sup> cm<sup>-3</sup>), storing enough energy to generate, upon electronic relaxation, strong chemical, structural and thermodynamic material evolutions. A processing feature is thus created, as illustrated in Fig. 1(a); a modified material voxel. This comprises first a change of the material dielectric function, and thus of its local optical properties and will represent one of the main topics to be discussed in the chapter. The replication of the focal spot in space and the combination of different scan strategies as shown in Fig. 1(b) can determine a 3D pattern of energy deposition and a complex geometrical assembly of structures with the creation of an optical function. The process, highlighting the strong energy localization by ultrashort laser pulses, was demonstrated in several pioneering works published at the end of the 90's by Davis *et al.* [1], Miura *et al.* [2] and by Glezer and Mazur [3], demonstrating the occurrence of positive refractive index changes in silica-based optical glasses for waveguiding applications and, respectively, strong void-like negative index changes potentially useful for data storage. This type of volume nanostructuring relied essentially on the control of the excitation level through the strength of focusing of the laser pulse, with moderate focusing generating soft index increase while a strong focusing enabling a complete breakdown of the material. The technique of ultrafast laser photoinscription based on refractive index engineering experienced, soon after, a strong development,

being nowadays a technology capable of uptaking new processing challenges well into the nanoscale [4, 5]. This roadmap driving laser processing on scales smaller than the optical wavelength leading to a super-resolved processing is the topic of the present chapter. The evolution of 3D ultrafast processing technologies towards miniaturization and packaging of several optical functions on a single chip and with a strong control of the achievable scale is expected to exert a strong impact on the field of photonics. Secondly, a change in the material implies both a variation of the structural bonding and arrangement. A variation of the specific volume generates expansion and thus mechanical movement. An actuator function emerges. Irradiated regions can thus develop new mechanical characteristics, a second application topic of this chapter.

Reviewing the achievements in terms of volume nanostructuring, the chapter will first discuss the basic principles defining optical and processing resolution. Approaching different types of photoinscription results and their thermodynamic conditions, it will then revisit several milestones that define today the field of volume nanostructuring, the process of micro-explosion in direct focusing conditions, the process of self-organization in embedded nanopatterns, the nonlinear generation of structural and chemical changes in nanoscale domains. Several applications will be reviewed at the end, relying on the use of nanoscale processing features to process and sample optical signals, among these, Bragg grating sensors, astrophotonic spectro-imagers, nonlinear frequency generation in crystalized glasses, or data storage. The fabrication of micro and nanomechanical devices will be discussed.

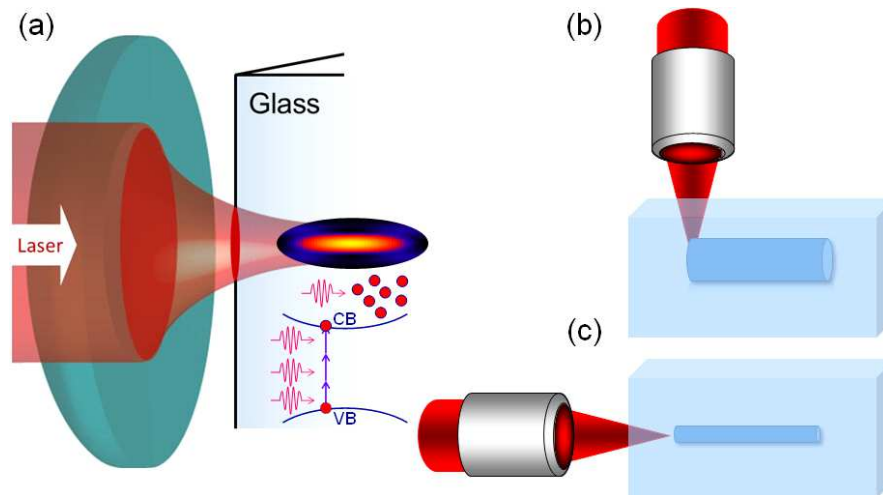


**Fig. 1** (a) The concept of nonlinear laser volume nanostructuring using focused ultrashort laser pulses. (b,c) Different scan strategies for volume photoinscription. Adapted with permission from [6] ©Springer Nature. Complex optical functions in three dimensions can be generated by combining the different irradiation geometries [6]. Extrapolating these features, other functionalities beyond the field of optics may be achieved.

## 2 The laser process

### 2.1 Optical resolution

The capability of generating optical functions relates to an accurate control of the magnitude and of the scale of the refractive index change. This capability of precise structuring has consequences that extend naturally beyond the optical field, to all emerging applications as the majority of generated functions depends on the scale of processing. Let us first focus on the latter and discuss the potential scales in volume structuring. An ultrashort laser pulse (e.g. 100 fs) of spectral bandwidth  $\Delta\omega$  and of field  $\mathcal{E}(t) \approx \int_{-\infty}^{\infty} \tilde{\mathcal{E}}(\omega)e^{i\omega t} d\omega$  passing through a focusing optical element is characterized in the focal plane mostly by its pulse duration and its spatial dimension [7]. Its multicolor wavepacket nature puts forward additional challenges in order to preserve the spatio-temporal characteristics up to the point of impact. In interaction with a transparent solid, these values define the local intensity profile and determine an intricate sequence of propagation and excitation events leading to a permanent modification of the material. This occurs only when the intensity is high enough to generate electronic excitation and to deposit energy at a level above the material modification threshold.

Already recognized in early works of imaging and microscopy of E. Abbe [8] and Lord Rayleigh [9], focusing light encounters the limit of diffraction. Following Rayleigh's concept, an optical plane wave can be focused down to a minimum Airy spot size (radius) of  $w = 0.61\lambda/NA$ , with  $NA$  being the numerical aperture and  $\lambda$  the optical wavelength. As the typical output of a laser system (the lowest order transverse mode) is a Gaussian beam and for optical systems with input pupils comparable to the beam dimension, we can approximate the spot profile with a Gauss function of waist  $w$  as  $I = I_0 \exp(-2r^2/w^2)$ , with  $r$  being the radial coordinate. Thus, for an optical system of  $NA \simeq 1$  (a system that combines resolution power and working distance) the lateral optical resolution is roughly  $\lambda/2$  and the axial resolution, approximated by the confocal distance is  $\pi\lambda/2$ . Different focusing configurations are depicted in Fig. 2(a), outlining the lateral spread of energy. The energy is then deposited within a domain given by the optical characteristic length estimated by a volume of  $\pi^2\lambda^3/8$ , energy diffusion from the interaction area, either thermal or electronic, being negligible for a dielectric material.

It has to be noted that volume interaction involves a propagation that, as intensity increases, becomes nonlinear culminating at the focal point with nonlinear electronic excitation. An intensity dependent nonlinear propagation will trigger, above a critical power level (in the range of few MW), self-focusing [10] and the early development of a carrier plasma that will follow in a first approximation a multiphoton ionization process. Due to the presence of carriers the self-focusing process stops, the beam collapse is arrested [11], the pulse divergence changes and the propagation becomes quasi-filamentary [12], a situation sketched in Fig. 2(b). These aspects are discussed to a great extent in Chapter 21, and the fundamental bases are reviewed in Chapter 1.

If the excitation leading eventually to permanent modification regimes lies at the border between perturbative and strong field processes (see recent reviews of the topic in [6, 13]), we will only retain here for the purpose of the argument two probable evolutions of the excitation profile; a multiphoton-induced narrowing of the profile and a filamentation-induced profile broadening. We note first a potential narrowing of the excitation profile following multiphoton ionization  $N_e \sim I^k = (I_0 e^{-\frac{2r^2}{w^2}})^k$ , with  $k$  being the multiphoton order (the number of photon quanta  $h\nu$  required to bridge the gap  $E_{gap}$ ), and for excitation levels (carrier densities) that do not strongly defocus the light. The new waist becomes  $w/\sqrt{k}$ . Secondly, with the emergence of carrier plasmas in excess of  $10^{16} \text{ cm}^{-3}$ , the carriers oscillating in the field form a negative lens that follows the spatial profile of the carrier density ( $\Delta n \sim N_e(r, t)$ ) modifying the field as  $\partial\mathcal{E}/\partial z \sim N_e\mathcal{E}$  [12]. As a side note, it is worth mentioning that carrier defocusing was one of the main reasons for which bulk modification was not observed in low focusing single pulse conditions (often applied in surface processing), as they may require higher numerical apertures ( $NA > 0.1$ ) and increased doses. The process may be exacerbated by materials with small electronic effective mass [14], for example a range of semiconducting materials. With the developing of the carrier plasma, the profile of excitation flattens and the characteristic scale increases, with the process depicted in Fig. 2(b,c). It is evident from the above considerations that optical resolution alone can hardly provide structural features smaller than 500 nm.

In order to achieve high processing resolutions [15], i.e. small structural features at a high density in space, a different process comes into play. The processing resolution, being related to the onset of a material structure, is in this case determined by a material or an observation threshold. The excitation will produce an observable permanent effect if on one hand the energy stored in the electrons matches a structural or thermodynamic threshold of the material (and the required carrier densities in this case are in the range of the critical density  $N_e \simeq 10^{21} \text{ cm}^{-3}$ ) or the energy deposition gradient, on the order of  $\rho_E/w$ , with  $\rho_E$  being the energy density, is sufficient to generate a thermomechanical effect leading to the failure of the material. In this case the processing resolution can be significantly smaller than the optical resolution. The condition that the energy associated with the excitation exceeds the material threshold requires consideration on the focusing strength and on the locally achieved intensity as the pulse wavepackets is affected by chromatic and geometric distortions as it crosses the optical elements and dielectric interfaces [16].

## 2.2 Photoinscription regimes

The nonlinear focusing and propagation of ultrashort laser pulses within a transparent material has multiple consequences on the spatial domain where optical energy is deposited in the material. The nonlinear excitation quantity, i.e. the free carrier population seeded by multiphoton or field ionization processes and multiplied in collisional events between accelerated electrons and atoms renders the photoinscription

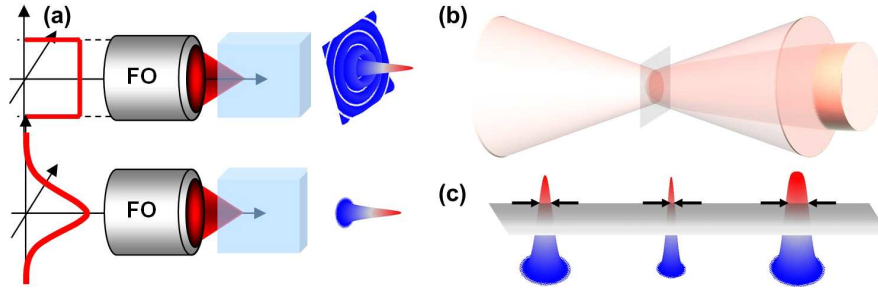


**Fig. 2** (a) Different focusing geometries and relative beam dimensions with respect to the pupil generating Airy and Gauss patterns. (b) Nonlinear beam propagation with a change in the beam divergence due to the onset of self-action and excitation processes. The divergence in a linear regime is shown to guide the eye. (c) Typical excitation profiles; Gaussian (left), power function of a Gaussian profile (middle), a flatten profile through defocusing (right). They correspond respectively to linear interactions, multiphoton processes, and carrier defocusing. The modification threshold is shown as a planar domain, signaling the excitation level from upon which the modification occurs. The resulting above-threshold modifications have smaller sizes than the respective optical beams for the first two cases, giving high accuracies. On the other hand, defocusing delocalize energy increasing the feature size while self-limiting the energy content and thus the strength of the interaction. This provides a stable but less resolved soft interaction regime.

process a predictable, deterministic character, equally observed in the processing results. This implies that the level of excitation does not fluctuate, being set by the seeded carriers and not by randomly localized absorption centers. Based on the morphological aspects of the laser affected zones we can first distinguish between (a) soft positive index changes and (b) strong negative index changes. Specific situations may appear where the two of them cohabit within the same spatial region.

### 2.2.1 Positive refractive index changes

The process is primarily based on a concept of bond-breaking and structural reorganization of matter [1, 17, 18] in spatial patterns defined by nonlinear propagation [19, 20], and will be discussed in Chapter 21. It lies at the base of volume waveguide photoinscription [1]; an image of a corresponding waveguide being given in Fig. 3(a). A bond-breaking event represents an increase of the bonding length (for example the  $Si - O$  bond in a silica-based glass) and occurs following an electronic excitation event which screens the charge and lowers the bonding strength. The consequence is a change in molecular polarizability and a certain structural flexibility where atoms can move to stabilize the internal energy of the molecular ensemble and to accommodate the charge redistribution. A strongly polarizable dielectric such as quartz or fused silica with strong electron-vibrational coupling will facilitate the process via the formation and the subsequent self-trapping of excitons in deformation potentials [21]. Such an electronically-induced process occurs primarily at low excitation levels in conditions of intensity clamping [22, 23], where the excitation

level (carrier density) is stabilized by a balance between self-focusing and defocusing in a range of  $10^{19} - 10^{20} \text{ cm}^{-3}$ . Thus implies a self-limiting process where any attempt to increase the carrier population via an intensity rise with a non-monotonic profile will accelerate light defocusing, reducing the intensity and decreasing the excitation yield, stabilizing the free carrier density and profile and regulating the interaction between carriers and the matrix. The follow up process can be declined in two correlated pathways; the generation of optical defects (broken bonds with charge compensation) and the reorganization of the matrix by rebonding (often in a denser state [17], as for example in a largely used support for photoinscription of optical functions; fused silica). This process, illustrated in Fig. 3(b), results in density and polarizability changes and can be associated to a weak index increase of about  $\Delta n \simeq 10^{-5}$  per laser pulse. Repetitive irradiation will thus generate useful index change values in the range of  $\Delta n \simeq 10^{-3}$  with a spatial scale related to the excitation profile in the  $\mu\text{m}$  range (Fig. 3(a)). Such an index change is called, inspired from Bragg gratings terminology, type I. Other effects may be equally considered for generating similar index values, namely mechanical densification and changes of the fictive temperature for optical glasses [24, 25] enabling molecular mobility (the sign of the index change depends of the standard or anomalous viscoelastic relaxation), or, provided that the laser repetition allows for an increase of the steady-state level of the temperature, ion-migration and changes of stoichiometry [26]. This regime of photochemistry-based photoinscription, first reported by Miura *et al.* [27] (and categorized here debatable as type I) was recently reviewed in [28]. An illustration of the process, indicating potential the migration of species is given in Fig. 3(c).

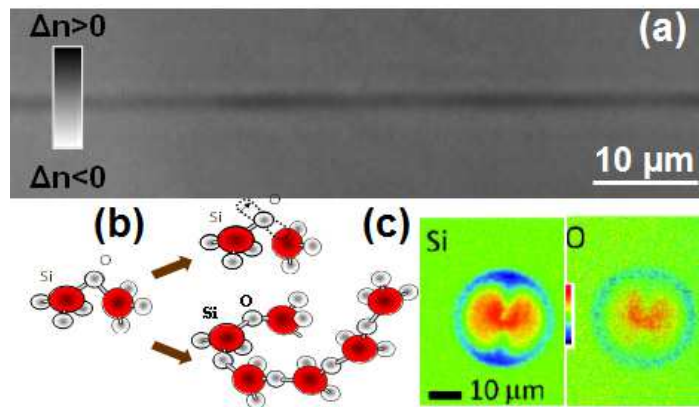


**Fig. 3** (a) Typical positive index change induced by moderately focused ultrashort laser pulses in fused silica (phase contrast microscopy image). The dark color indicates a positive change of the refractive index. (b) Schematic representation for bond breaking with defect generation and rebonding in smaller, hence denser, structural units, characteristic for fused silica [6]. (c) Heat-induced ion migration and stoichiometry changes in silicate glasses. Reprinted with permission from [26] ©The Optical Society.

To conclude, typical refractive index changes realized in this type I photoinscription regime and often reported for silicon oxide and silicate glasses are summarized in Fig. 3(a-c). The resulting index change is the base of laser fabrication of embedded optical waveguiding, essential for transporting and processing light [1, 29, 30, 31, 32, 33, 34, 35], and will be in detail discussed in Chapter 21. It is to be noted that in many cases, as a consequence of heat, the standard thermomechanical behavior will accompany the electronic changes via a counteracting thermomechanical expansion, and, if the initial host is a crystal, heating in a liquid phase and rapid cooling can generate local amorphisation, with the corresponding density, hence, refractive index change. Nonetheless, in optical glasses, the type I waveguiding is leading the conception of optical functions for transmitting, dividing or amplifying light. If the typical size is in the  $\mu\text{m}$  range, in combination with a chemical etching agent, the physical transformation can equally enable extreme nanometric scales. This situation will be discussed in Chapter 20, where nano-lithography concepts based on ultrafast irradiation and chemical etching selectivity will be discussed.

### 2.2.2 Strong negative refractive index changes

These types of index changes (called type II), with a much stronger contrast as the previous type appear once the energy concentration exceeds the mechanical stability of the solid. In this respect the process allows to fully benefit from a material threshold tuning the irradiation in the close vicinity and therefore to achieve a small feature size and, consequently, a high processing resolution. Thus, this index type and its characteristic scales will be the main concern of the present chapter. The energy requirements of this type of index change, obtained from more energetic inputs or tighter beam focusing conditions, come closer to the points of thermodynamic transitions or mechanical failure, suggesting that the energy density allows for the development of molecular decomposition, nucleation of gas bubbles, for the generation of material phases as dense plasma states or low viscosity states, or for exceeding the mechanical strength limit. All these evolutions are nevertheless intermediated by electronic excitation. Assuming that the energy per electron in the conduction band is limited by a collisional multiplication process at roughly 1.5 times the bandgap energy (up to 10 eV) [36], an estimation of the absorbed energy per unit volume will write as  $E_{abs} = N_e E_{gap}$ . This value of the absorbed energy density (equivalent to a local pressure), sustained by carrier densities in the range of  $10^{21} - 10^{22} \text{ cm}^{-3}$  should then approach the value of the bulk modulus (in the range of GPa) or determine at least a softening of the material with a temperature increase  $\Delta T = E_{abs}/c_p\rho$ , with  $c_p$  being the specific heat and  $\rho$  the material density. In these conditions several types of index change can appear, summarized in Fig. 4(a-d), with scales defined essentially by a material modification threshold.

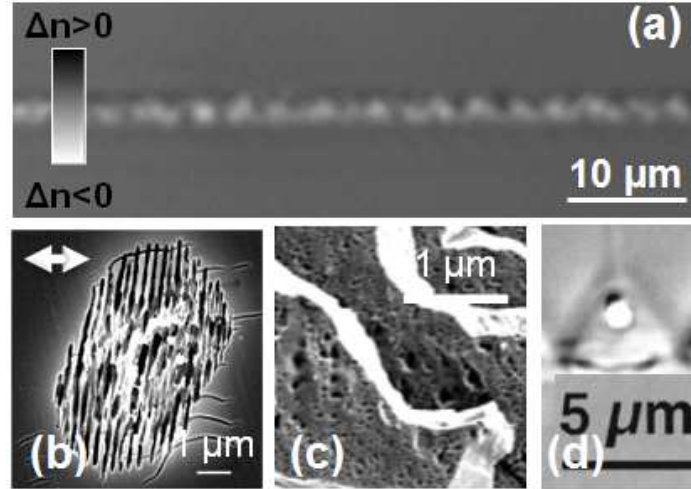


**Fig. 4** (a) Typical negative index change induced by focused ultrashort laser pulses in fused silica (phase contrast microscopy image). The light color indicates a decrease of the refractive index. (b,c,d) Different types of type II index change: (b) Generation of nanogratings in bulk fused silica, oriented perpendicular to the field. Reprinted with permission from [37] ©The Optical Society. (c) Generation of nanopores in fused silica in conditions of nanogratings formation. Reprinted with permission from [38] ©Wiley. (d) Generation of nanovoids via volume micro-explosion. Reprinted with permission from [39] ©American Institute of Physics.

### 2.2.3 Genesis and control of nanogratings

In 2003, Shimotsuma *et al.* [40] observed a new form of self-organization of matter in laser irradiated bulk fused silica in the shape of field-oriented periodic patterns of low index layers with a periodicity of approximately  $\lambda/2n$ , with  $n$  being the refractive index. This first report on nanogratings generation is illustrated in Fig. 5(a), showing a periodic arrangement perpendicular to the optical field polarization axis. The process corresponds to rather strong excitation conditions just under the void formation threshold, with possible generation of plasma waves [40]. Subject of strong interest from the laser-processing communities (see [41] for a review), these nanogratings emerged as an enabling morphological feature that generates anisotropic optical properties such as form birefringence and directional scattering [42, 43] as well as selective etching properties [43]. Their formation mechanism and the capacity of self-organization within a volume triggered equally a strong interest. The original plasma wave hypothesis [40] was not reconcilable with the currently reported electron densities and energies, requiring much stronger excitation conditions to form nanogratings. The formation of planar nano-layers was associated with the deformation of nanoplasmas initiated at defect based nucleation centers [44] in the intense optical field. Structural studies on the periodic layers indicated strong bond-breaking events [18] liberating the oxygen atoms and generating oxygen deficit in the structures (Fig. 5(b), oxygen-deficiency centers indicating the formation of inter-

nal interfaces), as well as the onset of nucleated pores of molecular decomposition [38] (Fig. 4(c)). These observations permitted to link the spatial development of the electric field with the morphological appearance of the modified material [45], determining the local field arrangement. Accounting for the subsequent generation of nm-scale roughness and volume centers (most probably few nm scaled voids generated by nucleation events or superposed micro-explosion events) that can scatter light generating periodic field and thus excitation patterns [46, 47], recent theoretical models proposed the onset and growth of ordered nanostructures as an interplay of interference of scattered light in near and far-fields with the evolution of plasma seeds [43] and the feedback-assisted growth of morphological features in low viscosity domains [48]. Local breakdown and cavitation conditions appear in nm-scale layered zones due to directional scattering, coherence, and near-field enhancement. The increase in the field values takes the form of a regular pattern aligned perpendicular to the field, source of cavitation in the high field zones and densification in between. With the dose, the order parameter increases and stabilizes. Fig. 5(c,d,e) depict the simulation results on the onset of ordered excitation layers (Fig. 5(c) [49]), experimental detection of evolution stages for nanostructure generation via X-ray scattering measurements (Fig. 5(d) [50]), the transformation from inhomogeneities to periodically-aligned nanorods [51] (Fig. 5(e)), and the theoretical description of the process [48] (Fig. 5(f)), illustrating the evolution from random inhomogeneities to fully-grown ordered nanogratings. Based on the mutual influence exercised dynamically between light and evolving matter including the competition between light near-field confinement and energy transport, the current model explains the multitude of organisational features within the pattern, including the orientation and the evolution of the periodicity towards smaller values [52]. The capability to observe experimentally the formation of nanostructures using X-ray scattering, electron microscopy, and optical diffraction, and to deliver a theoretical frame reproducing the observations represent essential steps into the understanding of a complex physical mechanism dynamically coupling light and matter and the way it can gradually determine their mutual evolution. Light triggers morphological modifications which in turn will reshape light patterns, pushing forward a material self-organisation process under light. The flow and dissipation of energy in such dynamical systems and their associated patterns will further reshape and reorganize matter. Within this frame, a common mechanism of organization was identified between surface and volume ordered nanostructures [53], as discussed in Chapter 5.

Recently, the control of such structures became so accurate that single nanoscale features can be induced using near-field enhancement features in diffuse media such as porous glass [55] or even in uniform media [57, 56], with dimensional scales in the range of tens of nm. The process is illustrated in Fig. 5(g,h). The key element here becomes the directional scattering and the positioning of the near field spots created by subsequent interference initiated by the intrinsic glass porosity or by existing structures that scatter light. A local cavitation or fracture event in the zone of field concentration enables feature scale in the 10 nm range.

The dependence on laser polarization as well as the dependence on the excitation conditions can be exploited in further nanogratings control experiments, either

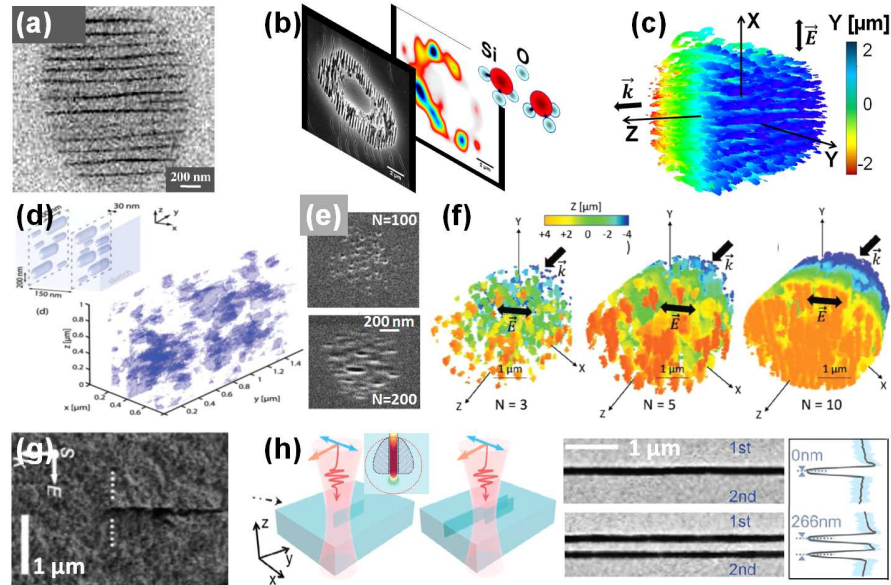


**Fig. 5** (a) Electronic microscopy image of volume nanogratings. Reprinted with permission from [40] ©American Physical Society. (b) Correlated distribution of nanogratings (electron microscopy image) and luminescence charts of oxygen deficiency centers [54] signaling internal interfaces and roughness. (c) Simulation distribution of layers of electronic charge. Reprinted with permission from [49] ©American Institute of Physics. (d) Tomography of nanogratings. X-ray scattering and imaging of bulk nanostructures. Reprinted with permission from [50] ©Wiley. (e) Gradual development of nanogratings from isolated inhomogeneities to periodically aligned nanorods with increasing photon dose. Adapted and reprinted with permission from [51] ©Springer Nature. (f). Simulated formation of nanogratings with increasing order. Reprinted with permission from [48] ©Wiley. (g) Single nanogratings feature generated in porous glass. Reprinted with permission from [55] ©The Optical Society. (h) Near-field mediated singular nanoscale features (irradiation sketch and image of results). Reprinted with permission from [56] ©Wiley.

by spatial polarization control [58], by mastering the level of excitation via pulse temporal design [59], via multipulse polarization experiments [60], or by directing the heat flux in relation to the scanning directions [61]. On one hand, non-standard beams with spatially defined polarization, for example azimuthal or radial beams but also beams with arbitrary defined polarization distribution, will then imprint their field structure on the processing result [58], with the local polarization defining the orientation of the nanolayers aligned perpendicular to the field. Circular polarization will generate twisted dot-resembling structures [62], adding chirality. On the other hand, the dispersion design of the laser beam, its chromatic control as well as mixing different colors would enable additional flexibility in defining the order degree or the period, and as such, the associated retardance. Maclair *et al.* [59] proposed an open loop pulse duration control associated with a feedback response derived from a diffracting UV beam to increase the nanogratings arrangement order by stretching the pulse in time or by the use of double pulse sequences. Shimotsuma

*et al.* [60] propose a synchronized double pulse polarization experiment to control the orientation generated by the nanogratings. Using multiple sequences of pulse pairs with orthogonal polarizations and variable interpulse delay in the ps range they demonstrated to achieve controllable retardance. Multicolor multipulse experiments as used for surface nanoscale periodic patterning [63] may be equally beneficial for bulk nanogratings. If these experiments address the control of the local electric field and excitation yield, energy flow in the sample and transport around excitation anisotropies may provide an additional control knob. A directional heat-transport model accounting for anisotropic heat diffusion in the presence of polarized optical fields was proposed by Stankevič *et al.* [61], intermediated by a direct coupling of the plasma electrons to the laser-field to give an additional orientational shift to nanogratings. Ponderomotive torques generated by wavefront tilts were equally suggested to contribute to the orientation of nanogratings [64]. Several examples are depicted in Fig. 6(a-d) showing respectively spatial field polarization control [58], (Fig. 6(a)), control via temporal tailoring [59] (Fig. 6(b)), double pulse polarization control [60] (Fig. 6(c)), and directional heat flux control [61] (Fig. 6(d)). Techniques of temporal and spatial control [65, 66] as those revisited in Chapter 15 and Chapter 17 have the potential to develop intelligent nanoprocessing techniques assisted by modern machine learning algorithms.

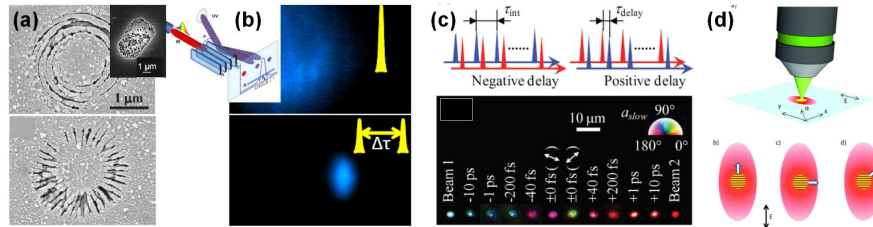


**Fig. 6** (a) Radial and azimuthal field imprinted nanogratings. Reprinted with permission from [58] ©American Physical Society. Inset: nanogratings imprinted by circularly polarized pulses [37]. (b) Observation and control of nanostructures induced by temporally tailored irradiation using diffraction feedback [59]. (c) Double pulse control of nanogratings with rotation of the slow axis. Reprinted with permission from [60] ©Wiley. (d) Schematic description of anisotropic heat flow generated by the coupling of the electron plasma with the laser field. Reprinted with permission from [61] ©Springer-Nature.

In the discussion above, the nanogratings structures involved strong negative index modulation with equally strong scattering properties. It is therefore important to note that ordered structures were also obtained in less invasive conditions for the material i.e. in a more gentle fashion, generating strong-enough birefringence with lower scattering losses [51]. These are based on intermediary formation stages resulting less pronounced nanostructured domains. The potential impact in applications will be discussed in the applications sections.

### 2.2.4 Genesis of single nanovoids

The original method for the fabrication of embedded void structures (voxels) relied on the concept of micro-explosion [3, 39] that underlined the achievement of high pressure, high temperature domains in the focal zone under tight focusing conditions. Building on this concept, Juodkazis *et al.* [67] indicated the generation of nanoscaled (in the 100 nm range) voids as the consequence of TPa electronic pressures achieved in the bulk [68] and the resulting shock, estimating the achievable scale from an energy conservation law implying that the internal energy within the shocked domain equals the absorbed energy. The void appears whenever the generated pressure exceeds the mechanical strength of the material. As such a cubic root relation can be determined between the size of the void and the amount of the absorbed energy  $D \simeq \sqrt[3]{E_{abs}}$ , suggesting the potential to obtain extremely small scales. Hydrodynamic simulations using QEOS and SESAME equations of state [68] supported the shock and failure scenario via an intermediate plasma state. The process is illustrated in Fig. 7(a,b), showing the resulting voids in different materials (experimental data and simulation results). This scenario demonstrates that the scale of the induced feature can be much smaller than the optical scale when intermediated by a material thermomechanical response. Within this range, in the neighbouring areas, the extreme thermomechanical conditions can be the birthplace for generating new densely-packed structural phase [69] by overcoming steric hindrance in the densification process (see also Chapter 13).

An important development in the nanoscale void generation technique relies on the extrapolation to one dimensional geometries as demonstrated by Bhuyan *et al.* [74, 75] in fused silica glass using non-diffractive Bessel-Gauss beams with high cone angles or dispersion control. This topic is discussed in detail in Chapter 16, which underlines the potential of conical waves to sustain nonlinear and geometrical distortions. A conceptual example is given in Fig. 7(c). The level of the energy deposition and its gradient can be controlled via a spatio-temporal design of the laser pulse. It is to be noted that, if the mechanical strength of the solids should be exceeded in order to generate a void-like structure, the condition can be relaxed if a transition towards lower viscosity states (e.g. liquid states) occurs first. This seems to happen in strongly-coupled and polarizable glasses (e.g. fused silica) and the nature of the process can be determined based on its characteristic times; tens, hundreds of ps for void generation in the solid [67] vs tens, hundreds of ns for void generation in the liquid [76]. This fact underlines a competition between the development of mechanical waves and the rapid achievement of liquid states with rapidly varying viscosities by a fast, potentially sub-ps, vibrational activation. For the latter process, a cavitation phenomenon is at work and defines the ultimate scale of the structural feature to tens of nm. Following spall and cavitation criteria defined by D. E. Grady [77] requiring that the elastic energy surpasses the cohesion energy, the process proceeds, limited by the speed of sound, to achieve a characteristic scale  $s = 2ut_{rest}$ , with  $u$  being the speed of sound and  $t_{rest}$  being the relaxation time. A discussion about possible process times and the corresponding resolution was recently given in [78]. It is to be noted that the thermomechanical conditions for cavitation, and

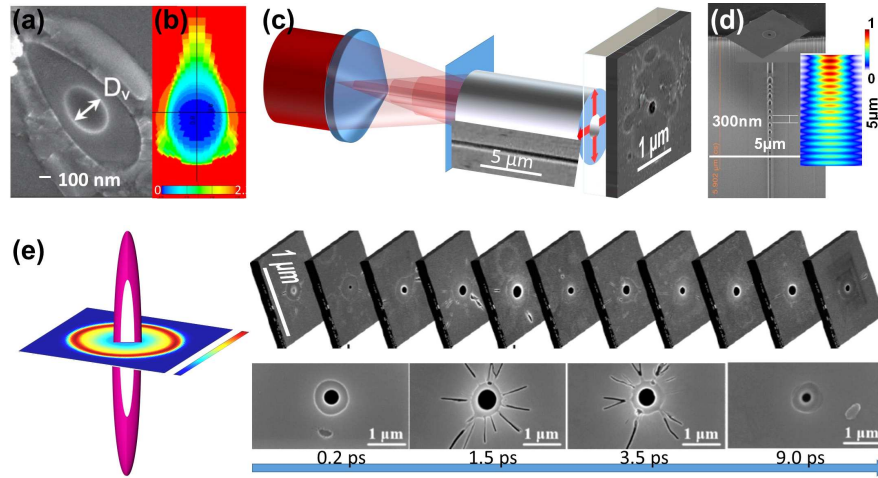


**Fig. 7** (a) Void generation in sapphire using tightly focused ultrashort laser radiation. Reprinted with permission from [67] ©American Physical Society. (b) Simulation of density redistribution in fused silica at 600 ps after excitation. The void is formed. Reprinted with permission from [68] ©American Physical Society. (c) Bessel-Gauss beam generation of one-dimensional voids. (d) Counterpropagating beam interference along the Bessel trace and the formation of nanovoid arrays. Reprinted with permission from [70] ©Wiley. (e) Reconstruction of the void and of the affected regions around the voxel with possible cracking under stress [71, 72]. Inset: 2D Compressive stress simulations around a laser-induced heat source. Adapted and reprinted with permission from [73] ©American Institute of Physics.

namely the achieved temperature in the 3000-4000 K range, are inferior but close to those corresponding to the rapid nucleation of a gas phase by vaporization [78]. The specific irradiation conditions enable further light confinement options. For example, in the vicinity of an interface, the superposition and synchronization of forward and back reflection will enable counterpropagating beam interference generation of nanocavities along the axis. The process, illustrated in Fig. 7(d) [70], is similar to the first reported array by Kanehira *et al.* [79].

If the processes mentioned above define the size of the laser-induced structures to well bellow the optical limit, a relevant question relates to the packaging density of such structuring features, i.e. how many nanoscale individual features can be grouped together on a surface unit. The self-organization strategies allow to stitch nanostructured domains almost seamlessly on large areas or volumes. However, the strategies for voxel generation, based on extreme thermomechanical conditions, inherently generate mechanically strained areas around the voxel with possible crack generation, generating a limit for dense packing of voxels. If the surrounding area presents intrinsic structural defects or if the stress around the energy deposition volume caused by thermal expansion exceeds the fracturing threshold (a positive Poisson coefficient could create for example shear stress with material yielding) [73], cracking occurs, limiting the minimal distance between structural voxels without generating catastrophic fracture connecting the voids. Accurate pulse energy,

duration and positioning are required to reduce the affected region to a minimum size and increase the packaging density [72]. Possible control strategies to limit the affected regions are summarized in Fig. 7(e).

### 2.2.5 Photochemical transformations

The discussion above referred to changes in material density and polarizability generated by electronically-induced bond-breaking and extreme thermomechanical effects. The laser-enabled material transformations in domains smaller than the characteristic optical scales are far more numerous, occurring again as a combination of nonlinear excitation and material threshold. In many cases the resulting transformation is directly related to the use of materials specifically designed for certain operations. Ultrafast laser irradiation of silver-doped glasses determines the formation of Ag clusters and nanoparticles, as it is discussed in Chapter 19 that reviews laser nanoscale photochemistry. The use of structured light inspired by the present super-resolution microscopy techniques enables the photochemical transformation on extreme scales [80]. The laser-enabled photochemistry can equally be used as a triggering step to nucleate crystallisation sites, stabilized then by thermal treatment, for example in photo-thermo-refractive glass [81]. Glass containing nanocrystals can exhibit anisotropic properties, and ultrafast laser radiation can selectively precipitate oriented nanocrystals in 3D. Fan *et al.* [82] successfully generated oriented  $\text{LiNbO}_3$  nanocrystalline domains in  $34\text{Li}_2\text{O}-33\text{Nb}_2\text{O}_5-33\text{SiO}_2$  glass samples. Similarly, three-dimensional luminescent perovskite domains with low formation energy were photoinscribed in Cs, Br, Pb containing oxide glass [83]. Several examples of photo-chemistry-mediated laser nanostructuring are given in Fig. 8(a-d).

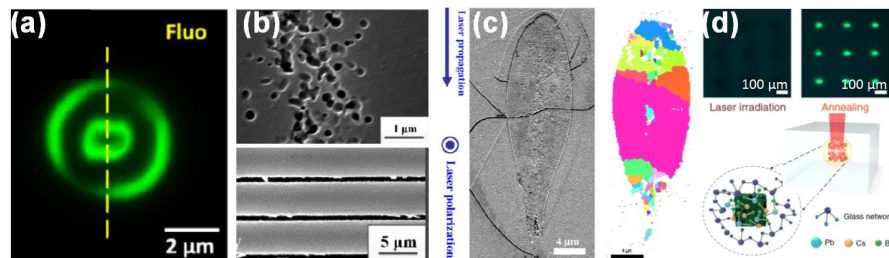


**Fig. 8** (a) Fluorescence patterns of silver clusters in silver-containing zinc phosphate glass. Reprinted with permission from [80] ©The Optical Society. (b) Nanocrystal sites in photo-thermal-glass enabled by ultrafast laser irradiation and thermal treatment [81]. (c) Precipitation of oriented  $\text{LiNbO}_3$  nanocrystalline domains in  $34\text{Li}_2\text{O}-33\text{Nb}_2\text{O}_5-33\text{SiO}_2$  glass. Reprinted with permission from [82] ©The Optical Society. (d) Luminescent perovskite domains laser photoinscribed in oxide glass matrix. Reprinted and adapted with permission from [83] ©Springer-Nature.

The photophysical, photostructural, and photochemical transformations were primarily linked to an optical function based on the local change of the dielectric

function. Their role extend nevertheless beyond optical functions and enable a rich taxonomy of functional features. The laser-induced polymorphism, the local changes in structure, in the chemical bonding, or in the specific volume will have consequences in tailoring mechanical properties (Young modulus, stress states), thermal and electrical transport features (heat and electrical conductivity) or etching selectivity. The coupling of these functional features allows to design sophisticated functional devices coupling optical, electrical thermal, and mechanical processes.

### 3 Applications of volume nanostructures in optics, photonics and micro-nano-mechanics

The capability to modify the volume of a transparent material had a strong impact in micro and nanofabrication techniques and related applications, adding to the generated function an intrinsic phase stability. For example, the optical function can be designed based on the structural evolution of matter and equally on the generation of thermomechanical effects (stress, cavitation, etc.) The build-up of an optical function in three-dimensional geometries can be seen as a specific type of additive manufacturing with subtractive features. The present state of the fabrication of embedded features in solid dielectrics for waveguiding using structural and stress-related features is reviewed in Chapter 21 as a technological platform for optical chips. The technique can extrapolated from solid to liquid environments. Photopolymerization using multiphoton absorption and the associated nanoscale features is discussed in Chapter 22. While giving some conceptual examples in Fig. 9(a–d), we will be concerned in the following with fabrication features that particularly address the nanoscale of laser-induced structural features in dielectrics with two main field of applications in view; photonics and nano-mechanics.

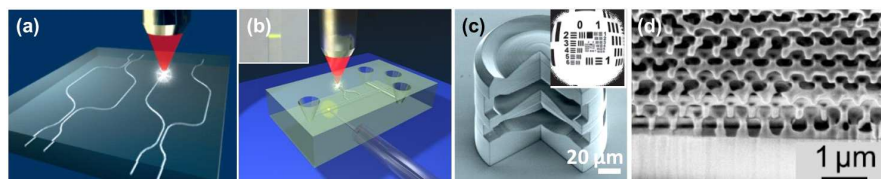


**Fig. 9** (a) Femtosecond laser photoinscribed optical circuit. Reprinted with permission from [84] ©Springer-Nature. (b) Ultrafast laser fabricated optofluidic chip. Reprinted with permission from [85] ©Wiley. (c) Micro-optics fabrication using direct laser writing of photo-polymerizable additive structures. Reprinted with permission from [86] ©Springer Nature. Inset: Simulated image of a resolution test chart. (d) Photonic crystal structure obtained by direct laser writing and photopolymerization. Reprinted with permission from [87] ©American Institute of Physics.

### 3.1 Photonics and optical technologies

Let us first, on the base of several example, illustrate the potential of ultrafast laser fabrication on extreme scales for photonics and optical technologies.

#### 3.1.1 Multifunctionality; micro-optics fabrication, nano-optics and nanofluidics

A dense packaging of nanoscaled bulk modification features creates a collective function originating in the periodic arrangement of structures. For example large domains structured with nanogratings enable an optical response sensitive to polarization as a type of form birefringence and anisotropic optical retardation. This optical response is partly similar to what can be expected from a mechanical stress reaction in the form of photoelasticity. This property was already recognized in the first report of Shimotsuma *et al.* [40]. A first consequence is to be observed in the manipulation of the wavefront of the crossing light leading to the fabrication of optical phase plates [88, 89, 90]. With a birefringence value in the range of  $\delta n_{oe} = 5 \times 10^{-3}$  for the visible range [42], phase retardance can be designed locally and generate wavefront engineering systems and phase retarders embedded in solid substrates [89, 90] or polarization gratings [91]. In combination to pulse front tilt, dichroism and chirality functions can be developed [64]. Cheng *et al.* [92] observed the polarisation sensitivity of type I waveguiding and selective division in fused silica associated with type II domains, where only polarization parallel to the nano-layers can be guided. Similar technique lead to the development of waveguide retarders [93]. Associated to optical fiber, the presence of nanogratings can generate controllable polarization effects [94, 95]. Another aspect should be mentioned here that will be developed in Chapter 20, notably the capacity to reach extreme scales by combining laser irradiation and chemical etching selectivity [96]. The dimensional scales enabled by laser structuring ( $d < \lambda$ ), the flexibility of arrangement in periodic patterns and the strong index contrast enable the development of optical resonances, the engineering of the dielectric function and of dispersion, and the control of the coherence, and, as such, the fabrication of optical bandgap and photonic crystal functions [97, 98]. Several examples relevant to these developments are illustrated in Fig. 10(a-e), resuming the fabrication of micro-optical elements and polarisation-sensitive waveguiding systems with modal control, transporting and manipulating light.

The nanoscale fabrication using nanogratings is not limited to optical fabrication; fluidic micro-systems belong to the potential field of applications (Fig. 10(e)). These will be discussed in Chapter 30. Similarly associated mechanical functions will be reviewed further below.

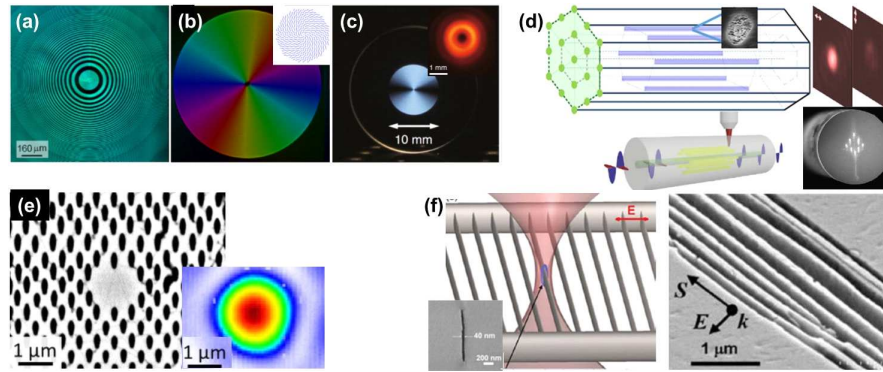


**Fig. 10** (a) Femtosecond laser photoinscribed Fresnel zone plate. Reprinted with permission from [88] ©The Optical Society. (b) Polarization converters based on nanogratings domains. Reprinted with permission from [88] ©The Optical Society. Inset: direction of nanogratings. (c) Low-loss birefringent wavefront converters. Reprinted with permission from [51] ©Springer Nature. Inset: generated vortex beam. (d) (top) Polarization large-mode area waveguides consisting of waveguiding traces and nanostructured domain. Evanescent coupling creates a polarized supermode [99]. (bottom) In-line fiber polarizer. Reprinted with permission from [95] ©Royal Society of Chemistry. (e) Light confinement and waveguiding in 2D patterns fabricated by ultrafast laser irradiation and selective chemical etching. Reprinted with permission from [96] ©Springer Nature. (f) (left) Nanofluidic device fabricated based on laser fabrication. Reprinted with permission from [100] ©De Gruyter. (right) Favorable direction of nanogratings for efficient etching. Reprinted with permission from [43] ©Wiley.

### 3.1.2 Data storage and quantum technologies

The generation of a local change of properties permits the inscription and the read-out of information using optical means. The scale achievable in bulk dielectric materials creates the premises of efficient data storage in a solid, resistant and protective environment. The first example, which will be developed to a large extent in Chapter 19, concerns the laser-mediated chemistry in doped materials, and, notably, the generation and aggregation of Ag atoms in photosensitive glass [101], leading to a high packing density of silver cluster dots embedded in the bulk, readable using third-harmonic generation microscopy. The advantages of this technique are related to the absence of bleaching, scattering, with directional read-out. The variability in the grey level of the read-out signal provides a four dimensionality to the memory support. With the emergence of laser-oriented nanogratings, a different technique of optical storage was proposed, exploiting a multidimensional space defined not only by the  $X, Y, Z$  position but also by the orientation of the slow axis and by the value of retardance, as proposed in 2014 by Zhang *et al.* [102]. The use of nanogratings bits allowed thus high capacity storage (potentially up to hundreds of TB per disc). Using the accurate control, similar data storage techniques can be applied to generate layers of field-oriented nanoslits with equivalent capacities [57, 56]. Besides the morphological aspects linking topography and storage function, laser-assisted structural transitions can further complement the range of data storage techniques with the gen-

eration of new structural phases. Going beyond the standard phase change materials, Huang *et al.* [83] utilised the laser-generated  $\text{CsPbBr}_3$  perovskite arrangements as reversible quantum dots in inorganic glassy matrices for optical storage and quantum technologies. To illustrate the results, several examples for data storage approaches based on laser micro and nano-fabrication are given in Fig. 11(a-d). Quantum applications foster equally laser techniques for the generation of qubits in quantum information processing systems or spin-based sensing applications. For example nitrogen vacancies (NV) in diamond were successfully reported using ultrafast laser techniques on surfaces and in the bulk [103, 104, 105]. The ultrashort laser pulse was found particularly effective to accurately position the centers in the bulk using pulse spatial control and particularly aberration corrections [105]. Recently, Hadden *et al.* [106] proposed a laser photoinscription method to generate both waveguiding systems and NV centers as a solution for quantum photonic networks. On a general basis, integrated quantum optical technologies [107, 108] will foster laser-based processing methods for all-optical fabrication including quantum sources, resonant systems and interconnects able to transport and manipulate photons in three dimensions [109, 110], and a range of laser micromachining applications for quantum photonics were recently reviewed [111] with the prospect of higher levels of miniaturization. It is worth noting that the potential of these techniques was recognized for high-end applications for example in cloud computing and media, coupling laser photoinscription and machine-learning-assisted information read-out, with ongoing efforts for development and commercialization [112].

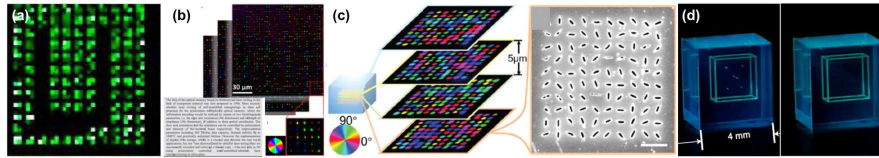


**Fig. 11** (a) Third-harmonic-generation readout of information bits generated by silver clusters in photosensitive glass. Reprinted with permission from [101] ©IntechOpen. (b) Multidimensional (5D) data storage in glass using nanogratings. Inset: retrieved document. Reprinted with permission from [102] ©American Physical Society. (c) 5D data storage using single slit-like features oriented in the field with electronic microscopy image of the modification layer. Reprinted with permission from [56] ©Wiley. (d) Reversible 3D structure of  $\text{CsPbBr}_3$  quantum dots in and inorganic glassy matrix. Reprinted with permission from [83] ©Springer-Nature.

### 3.1.3 Bragg waveguide sensors

A powerful field of applications for laser-induced volume nanostructures is the field of sensing and spectral filtering. The Bragg grating [113] insertable in a guiding element (e.g; fiber) represents a nanometer-scale periodic modulation of the refractive index, generating a resonant response (a coherent superposition of individual waves generated by the presence of periodic interfaces of different optical indices) at the

wavelength  $\lambda_B = 2n_{eff}\Lambda/m$ , with  $n_{eff}$  being the effective refractive index and  $\Lambda$  the pattern periodicity. This resonant response is defined by a spectrally selective retro-reflection peak or transmission dip, making Bragg gratings effective solutions for laser cavity design, spectral filtering or remote sensing [114]. The Bragg resonance is particularly sensitive to the variation of the effective index to external factors, making it a powerful sensor for detecting, for example, temperature and pressure variation (through thermo-optic and piezooptic effects), as well as the presence of ionizing radiation fields (via the generation of relevant optical defects and the associated opacity). The capability to confine light and harvest resolution indicates ultrafast laser pulses of different wavelengths as ideal sources for Bragg photoinscription. If usually interferometric techniques generating fringe patterns are applied [115, 116] to photoinscribe Bragg gratings by side illumination, more recently a direct irradiation technique was considered to take full benefit of the positioning capability of a focused ultrashort laser pulse [117]. The advances in the *point-by-point* techniques were comprehensively reviewed in a recent report by Ams *et al.* [118] illustrating also emerging applications. In this section we will pinpoint the most remarkable achievements in terms of the laser-induced modification scale indicating a range of relevant applications as illustrated in Fig. 12(a-g)). If the examples pertain mostly to optical glasses designed for the visible and near-infrared spectral region, the technique can be applied to a large variety of materials in crystalline and amorphous form. From the early developments of the point-by-point technique [117, 119], exploiting the precise positioning Bragg resonances were reported in waveguide bundles [120] (Fig. 12(a)). Slit shaping techniques [121] (elongation of the focal shape in one dimension in the Fourier plan by truncating the incident beam, giving a disk shape in the focal region) enabled the fabrication of planar patterns as Bragg gratings [122] (Fig. 12(b)). Strong reductions in the periodicity neighboring the 100 nm range were reported in tight focusing conditions allowing resonances in the visible range [118] (Fig. 12(c)). The positioning control including accurate synchronization between the laser source and the sample movement permits a variety of grating designs in terms of periodicity and apodization functions, controlling the spectral profile of the resonance. Examples of point-by-point laser techniques include non-standard fabrications such as: apodized [123], chirped [124], phase-shifted [125], or sampled gratings [126] (see [118] for a detailed discussion on various Bragg configurations achieved with fs laser pulses).

The spatial engineering of the beam enabled further progress. Controlled-aberrated filaments were used by Ertorer *et al.* [127] to generate elongated type II structures across an optical fiber (Fig. 12(d)). In order to obtain uniform, highly regulated arrays of one-dimensional voids crossing the core of a laser-fabricated embedded waveguide, Zhang *et al.* [128] used dispersion engineered non-diffractive Bessel-Gauss beams to fabricate high-resonance (40 dB/cm in fused silica) waveguide Bragg gratings (WBG) transiting towards the strong coupling regime (Fig. 12(e)), with the technique extendable to optical fibers (Fig. 12(f)). Multiplexing several WBGs on the same waveguide determine several concomitant resonances tuned across the telecom C-band spectrum [129]. Based on the index dependence of temperature (T) and strain ( $\varepsilon$ )  $dn = \frac{\partial n}{\partial T}dT + \frac{\partial n}{\partial \varepsilon}d\varepsilon$ , and a similar dependence of the pitch

(A), the resonance is sensitive to external conditions [130]. An indicative example of temperature measurement is given in Fig. 12(e). A 3D laser-fabricated sensor network was reported for measuring stress components [131, 132].

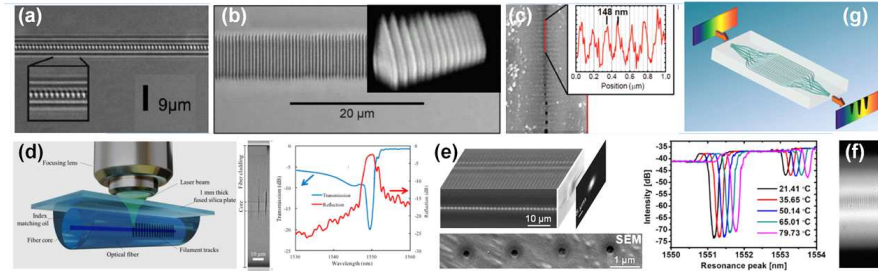


**Fig. 12** (a) Point-by-point dotted Bragg grating fabrication in a laser photowritten waveguide bundle. Reprinted with permission from [120] ©The Optical Society. (b) Point-by-point planar Bragg grating fabrication using slit-shaping of the focal region [121] in a laser photowritten waveguide. Reprinted with permission from [118] ©De Gruyter. (c) 100 nm range Bragg grating periodicity for the visible domain. Reprinted with permission from [118] ©De Gruyter. (d) Utilisation of aberrated filament-like beams for nanostructuring Bragg gratings in optical fibers. The reflected and transmitted spectra are given. Reprinted with permission from [127] ©The Optical Society. (e) Bessel-written waveguide Bragg gratings in laser-photowritten waveguides with strong Bragg resonances in fused silica [129]. The spectral resonance is sensitive to temperature due to a positive thermo-optic coefficient ( $10^{-5} \text{ }^\circ\text{C}^{-1}$ ) [128]. Reprinted with permission from [129, 128] ©The Optical Society. (f) Bessel-written waveguide Bragg gratings in an optical fiber. (g) Spectral filtering of multimode light using photonic lantern and waveguide Bragg gratings. Reprinted with permission from [133] ©Wiley.

With this example we point out an application field which is particularly large. The monolithic design of optical circuits and Bragg gratings permits to use different optical functions which show chromaticity (for example evanescent coupling in arrays or modal separation) in combination with spectral filtering. Spaleniak *et al.* [133] demonstrated narrow band spectral filtering of multimodal light in a 3D integrated optical chip using photonic lantern, with a conceptual design represented in Fig. 12(g), and potential applications in astronomy and chemical sensing of various chemical constituents in atmosphere [134]. Their spectral response enable the design of monolith waveguide lasers as distributed Bragg reflectors or gain elements [135]. The Bragg spectral response in connection to modal light transport permits the design of a variety of filters [136]. The ability to process optical signal can design not only optical chips but equally optofluidic chips and lab-on-chip detection systems enabling optical measurements of biochemical fluids [85, 137].

### 3.1.4 Optical field read-out in spectro-imagers; potential for astrophotonics

A powerful consequence of the nanometer sized cross-section of ultrafast laser-induced type II void-like changes and their close packing is the capability to sample

and read-out optical signals in optical circuits. The 100 nm size with sub-wavelength periodicities can be employed in the fabrication of embedded spectrometers that combine 3D design to augment collection efficiency and the high resolution given by the sampling rate. Standing-Wave-Integrated-Fourier-Transform-Spectrometers (SWIFTS) spectrometers [138] are prominent examples. The basic principle consist in the realisation of a standing field by superposing two replicas of the optical signal to be analyzed. Planar systems are already commercially available. A 3D geometry will improve the collection capacity in combination to other facilities in mode conversion, transport, or transformation, coupling imaging with spectral analysis. The nanoscale scattering centers will scatter light (depending on their arrangement as scattering centers or antennas to redirect signals towards a detector) containing the spectral information of the optical signal [139]. Their positioning will set the spectral resolution of the system. The as-designed dispositive is functional in various materials covering different spectral ranges [140]. A conceptual schema [141] with a practical realisation of a spectral detector is given in Fig. 13(a,b). The formalism and the basic principles of such systems are given in Chapter 28, which equally describe a range of applications. Such dispositive that integrate collection design via for example large aperture multimodal guides, modal transformations to single mode transport [142] can be applied for sensing and imaging celestial objects and their spectral signature in astronomy and astrophysics with a compact and robust astrophotonics design [143, 144, 145]. Their respond thus to a requirement of manipulating collection and processing weak optical signals coming from remote objects in space.

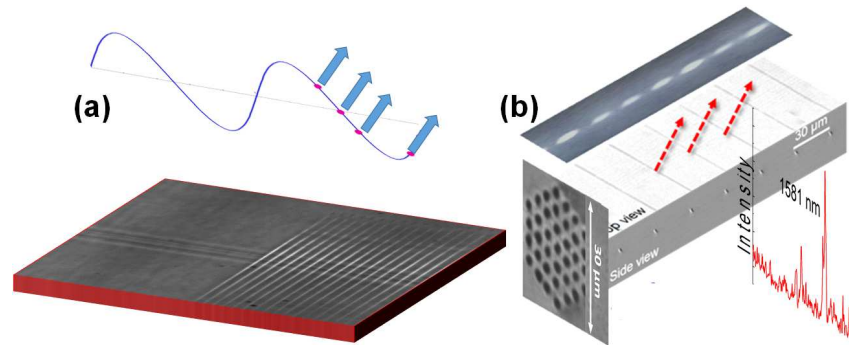


**Fig. 13** (a) Sampling the electrical field with nanoscale scattering centers. (b) Spectral detection using scattered radiation of standing patterns developed in the waveguide. Reprinted with permission from [141] ©The Optical Society. These concepts enable the design of embedded spectrometers and imagers.

### 3.2 Nanomechanics

Let us now review the laser-induced modifications from a different perspective, and we will shift the focus from the optical properties to micro-mechanical characteristics. As discussed in the previous sections and also in different chapters of this book, femtosecond laser exposure in a non-ablative regime induces permanent changes in the material structure. These laser-induced modifications can be of multiscale nature, starting from the molecular scale with the generation of defects and alterations in the molecular bonding, to mesoscopic scale with the formation of nanopores, cavities, and nanocracks of tens of nanometers, and all the way to micrometers scale bubbles resulting from the inner melting of the material. The nature of the laser-modification will inherently depend on the substrate material and on the laser-exposure conditions, and we have reviewed before the consequences for the refractive index design [1, 29, 40, 92] but briefly for the enhancement of chemical interactions and notably the selective nature of chemical etching [43, 146, 147, 148].

In fact, femtosecond laser pulses do change not only optical and chemical properties, but, by the bias of density changes and molecular bonding potentials, also properties such as the thermal transport (e.g. thermal conductivity) [152, 153], the Young modulus [154], and recently, thermomechanical properties, such as the coefficient of thermal expansion [149] and the Young modulus dependence with temperature [155]. One common effect is that these laser-induced modifications, be it of nanoscale or microscale, induce localized changes in the material physical properties, and chief of all, localized volume changes in the matter. The process is schematically represented in Fig. 14(a). Two important consequences emerge. The first one involves the fine positioning and control of mechanical movement with nm resolution [150], as illustrated in Fig. 14(b), showing an example of fine translation with its equivalent kinematics (a rotational effect is sketched in Fig. 14(c)). The second one involves the challenge to measure micromechanical changes on small scales. To circumvent the difficulty of quantifying thermomechanical changes in extremely small volumes that are often less than a micron-cube [156], a useful technique depicted in Fig. 14(c,d) is to use micro-machined cantilevers to amplify laser-induced changes into measurable displacement in the form of static deformation measurements [157] or frequency-resonance shifts, useful for investigating changes of elastic properties [155] and from here evolution laws. Using these methods, it was demonstrated that in fused silica, a regime of densification leads to a decrease of coefficient of thermal expansion, while the regime of nanogratings has the opposite effect [149]. Interestingly, it was also shown that the nanogratings, whose orientation is governed by the laser light polarization can be used to create direct-write composite in the material [155] and that this can be used to tune the Young's modulus dependence with temperature to an appreciable level [158]. These are just examples reported for femtosecond laser exposure of fused silica. Similar approaches can be used to investigate laser-induced physical properties changes in other material systems leading to a capacity to determine and measure mechanical properties of laser-modified materials.

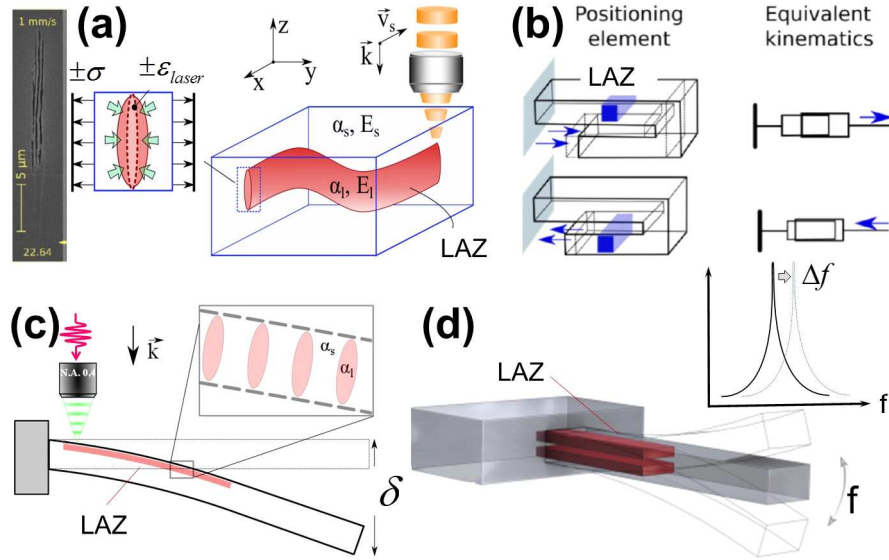


**Fig. 14** Controlling stress with nanogratings in micro-mechanical systems. (a) Illustration of laser-induced changes in thermomechanical properties. Local arbitrarily written laser-induced modification patterns (laser-affected zone LAZ) generate thermomechanical expansion, localized stress and structural modification, impacting mechanical properties. Via mechanical motion, these modifications determine nm-scale adjustments of position of micro-mechanical systems (actuator) Adapted from [149] ©American Physical Society. (b) Fine tuning mechanical translation and its equivalent kinematics. Reprinted from [150] ©The Optical Society. (c) Probing mechanical properties. Illustration of the use of micro-mechanical cantilever to probe thermomechanical changes in transparent materials. The tip displacement is measured by interferometry or by using triangulation optical sensing, similar to the methods used in atomic force microscopy. The material changes in terms of density and structural bonding generate variation in the mechanical evolution laws, affecting displacement and oscillation frequency. (d) Using cantilevers set in vibration, the monitoring of the natural frequency resonance after laser exposure can be used to access information related to the changes in the Young modulus. Reprinted with permission from [151] ©The Optical Society.

## 4 Conclusion and perspectives

This chapter, with its perspective stretching from optics to nanomechanics, outlined the present capability of ultrashort laser pulses to achieve extreme processing scales in bulk transparent materials where a three-dimensional geometry offers extended capabilities to collect, transport, process, and read-out light as well as high flexibility to determine and quantify mechanical evolution. An advanced optical design would then rely on the scale, on the geometry, and on the morphology change. This capability of laser processing is based on strong optical nonlinearities and focusing strength and, in parallel, on guided material reaction to light and energy gradients, being fueled by advanced beam spatio-temporal engineering techniques [15]. The thresholded material response to energy gradients can determine extreme feature scales in both direct and self-organized patterning under light. The periodic patterns

and the design of anisotropic and wavefront engineering functions follow already an industrial development. A similar industrial uptake concerns 3D optical circuits for remote sensing and telecom applications. High density optical storage and quantum technologies follow equally a swift development with radical progress in the controllability of the optical design and efficiency. To the mechanical side, the accurate control of structuring allows to design features and micro-mechanical devices to execute precise mechanical movements as well as to characterize mechanical properties on extreme scales.

The chapter has given several prominent examples of the current advances of laser volume nanostructuring, posing equally the fundamental question of the principle limits of structural modification sizes. Are there fundamental obstacles in pushing the limits of the scale and the self-organization periods beyond the standard scales defined by light? The 100 nm range, a cornerstone in laser processing is already achieved, with in view the 10 nm scale. Given the high resolution and in many cases resonant response, this milestone will enable photonic and sensing techniques in multispectral ranges and with high packaging density, as well as extended means of controlling and engineering light. Exciting opportunities in storing information for cloud computing or in quantum transport are underway. Combination of chemical and optical effects on the nanoscale will push forward the limits of nanostructuring towards a range of coupled functionalities, from sensing to fluidic transport. On the other end we equally face thriving prospect of controlling mechanical movement with extreme precision, coupling optical and actuating functions.

In parallel massive progress is achieved in observing the nanoscale [159]. With the implementation of in-situ rapid quantitative observation capacity, the concept of control will qualitatively reach a new level. Exploring a complex phase space of irradiation parameters, learning algorithms will help guiding laser processes towards the achievement of higher accuracy and yield, defining the base of smart laser nanoscale manufacturing. A challenging but rewarding pathway of laser extreme nanostructuring lies ahead, correlating scale to pattern, pattern to function, and function to application.

## References

1. K.M. Davis, K. Miura, N. Sugimoto, K. Hirao, *Opt. Lett.* **21**(21), 1729 (1996)
2. K. Miura, J. Qiu, H. Inouye, T. Mitsuyu, K. Hirao, *Appl. Phys. Lett.* **71**(23), 3329 (1997). DOI 10.1063/1.120327
3. E.N. Glezer, E. Mazur, *Appl. Phys. Lett.* **71**(7), 882 (1997). DOI 10.1063/1.119677
4. H. Misawa, S. Juodkazis, *3D Laser Microfabrication: Principles and Applications* (Wiley, 2006). DOI 10.1002/352760846X
5. K. Sugioka, Y. Cheng, *Light Sci. Appl.* **3**(4), e149 (2014). DOI 10.1038/lsa.2014.30
6. R. Stoian, *Appl. Phys. A* **126**, 438 (2020). DOI 10.1007/s00339-020-03516-3
7. M. Wollenhaupt, A. Assion, T. Baumert, *Femtosecond Laser Pulses: Linear Properties, Manipulation, Generation and Measurement* (Springer, 2007), p. 937. DOI 10.1007/978-0-387-30420-5-12
8. E. Abbe, *Arch. mikr. Anat.* **9**(1), 469 (1873). DOI 10.1007/BF02956177

9. L.R. F.R.S., Lond. Edinb. Phil. Mag. **8**(49), 261 (1879). DOI 10.1080/14786447908639684
10. J. Marburger, Prog. Quantum. Electron. **4**, 35 (1975). DOI 10.1016/0079-6727(75)90003-8
11. A.L. Gaeta, Phys. Rev. Lett. **84**, 3582 (2000). DOI 10.1103/PhysRevLett.84.3582
12. A. Couairon, L. Sudrie, M. Franco, B. Prade, A. Mysyrowicz, Phys. Rev. B **71**, 125435 (2005). DOI 10.1103/PhysRevB.71.125435
13. D. Tan, K.N. Sharafudeen, Y. Yue, J. Qiu, Prog. Mat. Sci. **76**, 154 (2016). DOI 10.1016/j.pmatsci.2015.09.002
14. V.V. Kononenko, V.V. Konov, E.M. Dianov, Opt. Lett. **37**(16), 3369 (2012). DOI 10.1364/OL.37.003369
15. R. Stoian, J.P. Colombier, Nanophotonics **9**(16), 4665 (2020). DOI doi:10.1515/nanoph-2020-0310. URL 10.1515/nanoph-2020-0310
16. J. Diels, W. Rudolph, P. Liao, P. Kelley, *Ultrashort Laser Pulse Phenomena*. Optics and photonics (Elsevier Science, 2006). DOI 10.1016/B978-0-12-215493-5.X5000-9
17. J.W. Chan, T.R. Huser, S.H. Risbud, D.M. Krol, Appl. Phys. A **76**(3), 367 (2003). DOI 10.1007/s00339-002-1822-9
18. K. Mishchik, C. D'Amico, P.K. Velpula, C. Mauclair, A. Boukenter, Y. Ouerdane, R. Stoian, J. Appl. Phys. **114**(13), 133502 (2013). DOI 10.1063/1.4822313
19. L. Sudrie, A. Couairon, M. Franco, B. Lamouroux, B. Prade, S. Tzortzakis, A. Mysyrowicz, Phys. Rev. Lett. **89**, 186601 (2002). DOI 10.1103/PhysRevLett.89.186601
20. I.M. Burakov, N.M. Bulgakova, R. Stoian, A. Mermillod-Blondin, E. Audouard, A. Rosenfeld, A. Husakou, I.V. Hertel, J. Appl. Phys. **101**(4), 043506 (2007). DOI 10.1063/1.2436925
21. P. Martin, S. Guizard, P. Daguzan, G. Petite, P. D'Oliveira, P. Meynadier, M. Perdrix, Phys. Rev. B **55**, 5799 (1997)
22. G.N. Steinberg, Phys. Rev. A **4**, 1182 (1971). DOI 10.1103/PhysRevA.4.1182
23. V.P. Kandidov, V.Y. Fedorov, O.V. Tverskoi, O.G. Kosareva, S.L. Chin, Quantum Elec. **41**(4), 382 (2011). DOI 10.1070/qe2011v041n04abeh014486
24. R. Brückner, J. Non-Cryst. Solids **5**(2), 123 (1970). DOI https://doi.org/10.1016/0022-3093(70)90190-0
25. L. Bressel, D. de Ligny, C. Sonnevile, V. Martinez, V. Mizeikis, R. Buividas, S. Juodkazis, Opt. Mater. Express **1**(4), 605 (2011). DOI 10.1364/OME.1.000605
26. M. Sakakura, T. Kurita, M. Shimizu, K. Yoshimura, Y. Shimotsuma, N. Fukuda, K. Hirao, K. Miura, Opt. Lett. **38**(23), 4939 (2013). DOI 10.1364/OL.38.004939
27. K. Miura, J. Qiu, T. Mitsuyu, K. Hirao, Opt. Lett. **25**(6), 408 (2000). DOI 10.1364/OL.25.000408
28. T. Fernandez, M. Sakakura, S. Eaton, B. Sotillo, J. Siegel, J. Solis, Y. Shimotsuma, K. Miura, Prog. Mat. Sci. **94**, 68 (2018). DOI 10.1016/j.pmatsci.2017.12.002
29. S. Nolte, M. Will, J. Burghoff, A. Tünnermann, Appl. Phys. A **77**, 109 (2003). DOI 10.1007/s00339-003-2088-6
30. D. Blömer, A. Szameit, F. Dreisow, T. Schreiber, S. Nolte, A. Tünnermann, Opt. Express **14**(6), 2151 (2006). DOI 10.1364/OE.14.002151
31. S.M. Eaton, M.L. Ng, J. Bonse, A. Mermillod-Blondin, H. Zhang, A. Rosenfeld, P.R. Herman, Appl. Opt. **47**, 2098 (2008)
32. L. Sansoni, F. Sciarrino, G. Vallone, P. Mataloni, A. Crespi, R. Ramponi, R. Osellame, Phys. Rev. Lett. **105**, 200503 (2010). DOI 10.1103/PhysRevLett.105.200503
33. R.R. Thomson, T.A. Birks, S.G. Leon-Saval, A.K. Kar, J. Bland-Hawthorn, Opt. Express **19**(6), 5698 (2011). DOI 10.1364/OE.19.005698
34. S. Gross, M.J. Withford, Nanophotonics **4**(3), 332 (2015). DOI doi:10.1515/nanoph-2015-0020
35. S. Minardi, G. Cheng, C. D'Amico, R. Stoian, Opt. Lett. **40**(2), 257 (2015). DOI 10.1364/OL.40.000257
36. A. Kaiser, B. Rethfeld, M. Vicanek, G. Simon, Phys. Rev. B **61**, 11437 (2000). DOI 10.1103/PhysRevB.61.11437
37. K. Mishchik, G. Cheng, G. Huo, I.M. Burakov, C. Mauclair, A. Mermillod-Blondin, A. Rosenfeld, Y. Ouerdane, A. Boukenter, O. Parriaux, R. Stoian, Opt. Express **18**(24), 24809 (2010). DOI 10.1364/OE.18.024809

38. M. Lancry, B. Pommellec, J. Canning, K. Cook, J.C. Poulin, F. Brisset, *Laser Photonics Rev.* **7**(6), 953 (2013). DOI 10.1002/lpor.201300043
39. C.B. Schaffer, A.O. Jamison, E. Mazur, *Appl. Phys. Lett.* **84**(9), 1441 (2004). DOI 10.1063/1.1650876
40. Y. Shimotsuma, P.G. Kazansky, J. Qiu, K. Hirao, *Phys. Rev. Lett.* **91**, 247405 (2003). DOI 10.1103/PhysRevLett.91.247405
41. B. Zhang, X. Liu, J. Qiu, *J. Materiomics* **5**(1), 1 (2019). DOI 10.1016/j.jmat.2019.01.002
42. P.G. Kazansky, Y. Shimotsuma, *J. Ceram. Soc. Japan* **116**(1358), 1052 (2008). DOI 10.2109/jcersj2.116.1052
43. R. Taylor, C. Hnatovsky, E. Simova, *Laser Photonics Rev.* **2**(1-2), 26 (2008). DOI 10.1002/lpor.200710031
44. V.R. Bhardwaj, E. Simova, P.P. Rajeev, C. Hnatovsky, R.S. Taylor, D.M. Rayner, P.B. Corkum, *Phys. Rev. Lett.* **96**, 057404 (2006). DOI 10.1103/PhysRevLett.96.057404
45. F. Liang, J. Bouchard, S. Leang Chin, R. Vallée, *Appl. Phys. Lett.* **107**(6), 061903 (2015). DOI 10.1063/1.4928551
46. R. Buschlinger, S. Nolte, U. Peschel, *Phys. Rev. B* **89**, 184306 (2014). DOI 10.1103/PhysRevB.89.184306
47. A. Rudenko, J.P. Colombier, T.E. Itina, *Phys. Rev. B* **93**, 075427 (2016). DOI 10.1103/PhysRevB.93.075427
48. A. Rudenko, J.P. Colombier, T.E. Itina, R. Stoian, *Adv. Opt. Mat.* **9**(20), 2100973 (2021). DOI 10.1002/adom.202100973
49. G. Cheng, A. Rudenko, C. D'Amico, T.E. Itina, J.P. Colombier, R. Stoian, *Appl. Phys. Lett.* **110**(26), 261901 (2017). DOI 10.1063/1.4987139
50. S. Richter, A. Plech, M. Steinert, M. Heinrich, S. Döring, F. Zimmermann, U. Peschel, E. Kley, A. Tünnermann, S. Nolte, *Laser Photonics Rev.* **6**(6), 787 (2012). DOI 10.1002/lpor.201200048
51. M. Sakakura, Y. Lei, L. Wang, Y.H. Yu, P.G. Kazansky, *Light Sci. Appl.* **9**(1), 15 (2020). DOI 10.1038/s41377-020-0250-y
52. S. Richter, M. Heinrich, S. Döring, A. Tünnermann, S. Nolte, U. Peschel, *Journal of Laser Applications* **24**(4), 042008 (2012). DOI 10.2351/1.4718561
53. A. Rudenko, J.P. Colombier, S. Höhm, A. Rosenfeld, J. Krüger, J. Bonse, T.E. Itina, *Sci. Rep.* **7**, 12306 (2017). DOI 10.1038/s41598-017-12502-4
54. R. Stoian, K. Mishchik, G. Cheng, C. Maclair, C. D'Amico, J.P. Colombier, M. Zamfirescu, *Opt. Mater. Express* **3**(10), 1755 (2013). DOI 10.1364/OME.3.001755
55. Y. Liao, J. Ni, L. Qiao, M. Huang, Y. Bellouard, K. Sugioka, Y. Cheng, *Optica* **2**(4), 329 (2015). DOI 10.1364/OPTICA.2.000329
56. Z. Yan, J. Gao, M. Beresna, J. Zhang, *Adv. Opt. Mat.* **10**(4), 2101676 (2021). DOI 10.1002/adom.202101676
57. Y. Lei, M. Sakakura, L. Wang, Y. Yu, H. Wang, G. Shayeganrad, P.G. Kazansky, *Optica* **8**(11), 1365 (2021). DOI 10.1364/OPTICA.433765
58. C. Hnatovsky, V. Shvedov, W. Krolikowski, A. Rode, *Phys. Rev. Lett.* **106**, 123901 (2011). DOI 10.1103/PhysRevLett.106.123901
59. C. Maclair, M. Zamfirescu, J.P. Colombier, G. Cheng, K. Mishchik, E. Audouard, R. Stoian, *Opt. Express* **20**(12), 12997 (2012). DOI 10.1364/OE.20.012997
60. Y. Shimotsuma, M. Sakakura, P.G. Kazansky, M. Beresna, J. Qiu, K. Miura, K. Hirao, *Adv. Mat.* **22**(36), 4039 (2010). DOI 10.1002/adma.201000921
61. V. Stankevič, G. Račiukaitis, F. Bragheri, X. Wang, E.G. Gamaly, R. Osellame, S. Juodkazis, *Sci. Rep.* **7**, 39989 (2017). DOI 10.1038/srep39989
62. R.S. Taylor, E. Simova, C. Hnatovsky, *Opt. Lett.* **33**(12), 1312 (2008). DOI 10.1364/OL.33.001312
63. S. Höhm, M. Herzlieb, A. Rosenfeld, J. Krüger, J. Bonse, *Applied Surface Science* **374**, 331 (2016). DOI 10.1016/j.apsusc.2015.12.129
64. B. Pommellec, M. Lancry, R. Desmarchelier, E. Hervé, B. Bourguignon, *Light Sci. Appl.* **5**(11), e16178 (2016). DOI 10.1038/lsa.2016.178

65. R. Stoian, M. Wollenhaupt, T. Baumert, I.V. Hertel, in *Laser Precision Microfabrication*, ed. by K. Sugioka, M. Meunier, A. Piqué (Springer Berlin Heidelberg, Berlin, Heidelberg, 2010), pp. 121–144. DOI 10.1007/978-3-642-10523-4-5
66. H. Zhang, S. Hasegawa, H. Toyoda, Y. Hayasaki, *Optics and Lasers in Engineering* **151**, 106884 (2022). DOI 10.1016/j.optlaseng.2021.106884
67. S. Juodkazis, K. Nishimura, S. Tanaka, H. Misawa, E.G. Gamaly, B. Luther-Davies, L. Hallo, P. Nicolai, V.T. Tikhonchuk, *Phys. Rev. Lett.* **96**, 166101 (2006). DOI 10.1103/PhysRevLett.96.166101
68. L. Hallo, A. Bourgeade, V.T. Tikhonchuk, C. Mezel, J. Breil, *Phys. Rev. B* **76**, 024101 (2007). DOI 10.1103/PhysRevB.76.024101
69. A. Vailionis, E.G. Gamaly, V. Mizeikis, W. Yang, A.V. Rode, S. Juodkazis, *Nat. Commun.* **2**, 445 (2011). DOI 10.1038/ncomms1449
70. P.K. Velpula, M.K. Bhuyan, F. Courvoisier, H. Zhang, J.P. Colombier, R. Stoian, *Laser Photonics Rev.* **10**(2), 230 (2016). DOI 10.1002/lpor.201500112
71. T. Chen, G. Zhang, Y. Wang, X. Li, R. Stoian, G. Cheng, *Micromachines* **11**(7), 671 (2020). DOI 10.3390/mi11070671
72. G. Zhang, R. Stoian, R. Lou, T. Chen, G. Li, X. Wang, Y. Pan, P. Wu, J. Wang, G. Cheng, *Applied Surface Science* **570**, 151170 (2021). DOI 10.1016/j.apsusc.2021.151170
73. R. Beuton, B. Chimier, J. Breil, D. Hébert, P.H. Maire, G. Duchateau, *J. Appl. Phys.* **122**(20), 203104 (2017). DOI 10.1063/1.4993707
74. M.K. Bhuyan, F. Courvoisier, P.A. Lacourt, M. Jacquot, R. Salut, L. Furfaro, J.M. Dudley, *Appl. Phys. Lett.* **97**(8), 081102 (2010). DOI 10.1063/1.3479419
75. M.K. Bhuyan, P.K. Velpula, J.P. Colombier, T. Olivier, N. Faure, R. Stoian, *Appl. Phys. Lett.* **104**(2), 021107 (2014). DOI 10.1063/1.4861899
76. M.K. Bhuyan, M. Somayaji, A. Mermillod-Blondin, F. Bourquard, J.P. Colombier, R. Stoian, *Optica* **4**(8), 951 (2017). DOI 10.1364/OPTICA.4.000951
77. D. Grady, *Journal of the Mechanics and Physics of Solids* **36**(3), 353 (1988). DOI 10.1016/0022-5096(88)90015-4
78. R. Stoian, M.K. Bhuyan, A. Rudenko, J.P. Colombier, G. Cheng, *Adv. Phys.-X* **4**(1), 1659180 (2019). DOI 10.1080/23746149.2019.1659180
79. S. Kanehira, J. Si, J. Qiu, K. Fujita, K. Hirao, *Nano Lett.* **5**(8), 1591 (2005). DOI 10.1021/nl0510154
80. K. Mishchik, Y. Petit, E. Brasselet, A. Royon, T. Cardinal, L. Canioni, *Opt. Lett.* **40**(2), 201 (2015). DOI 10.1364/OL.40.000201
81. Y. Zhang, X. Wang, G. Zhang, R. Stoian, G. Cheng, *Nanomaterials* **11**(6) (2021). DOI 10.3390/nano11061432
82. C. Fan, B. Poumellec, M. Lancry, X. He, H. Zeng, A. Erraji-Chahid, Q. Liu, G. Chen, *Opt. Lett.* **37**(14), 2955 (2012). DOI 10.1364/OL.37.002955
83. X. Huang, Q. Guo, D. Yang, X. Xiao, X. Liu, Z. Xia, F. Fan, J. Qiu, G. Dong, *Nat. Photonics* **14**(2), 82 (2019). DOI 10.1038/s41566-019-0538-8
84. F. Flamini, L. Magrini, A.S. Rab, N. Spagnolo, V. D'Ambrosio, P. Mataloni, F. Sciarrino, T. Zandrini, A. Crespi, R. Ramponi, R. Osellame, *Light Sci. Appl.* **4**(11), e354 (2015). DOI 10.1038/lsa.2015.127
85. R. Osellame, H. Hoekstra, G. Cerullo, M. Pollnau, *Laser Photonics Rev.* **5**(3), 442 (2011). DOI <https://doi.org/10.1002/lpor.201000031>
86. T. Gissibl, S. Thiele, A. Herkommer, H. Giessen, *Nat. Photonics* **10**(8), 554 (2016). DOI 10.1038/nphoton.2016.121
87. M. Thiel, J. Fischer, G. von Freymann, M. Wegener, *Appl. Phys. Lett.* **97**(22), 221102 (2010). DOI 10.1063/1.3521464
88. M. Beresna, M. Gecevičius, P.G. Kazansky, *Opt. Mater. Express* **1**(4), 783 (2011). DOI 10.1364/OME.1.000783
89. J. Tian, H. Yao, M. Cavillon, E. Garcia-Caurel, R. Ossikovski, M. Stchakovsky, C. Eypert, B. Poumellec, M. Lancry, *Micromachines* **11**(2), 131 (2020). DOI 10.3390/mi11020131
90. S. Xu, H. Fan, Z.Z. Li, J.G. Hua, Y.H. Yu, L. Wang, Q.D. Chen, H.B. Sun, *Opt. Lett.* **46**(3), 536 (2021). DOI 10.1364/OL.413177

91. M. Beresna, P.G. Kazansky, *Opt. Lett.* **35**(10), 1662 (2010). DOI 10.1364/OL.35.001662
92. G. Cheng, K. Mishchik, C. Mauclair, E. Audouard, R. Stoian, *Opt. Express* **17**(12), 9515 (2009). DOI 10.1364/OE.17.009515
93. L.A. Fernandes, J.R. Grenier, P.R. Herman, J.S. Aitchison, P.V.S. Marques, *Opt. Express* **19**(19), 18294 (2011). DOI 10.1364/OE.19.018294
94. C. Hnatovsky, D. Grobnic, D. Coulas, M. Barnes, S.J. Mihailov, *Opt. Lett.* **42**(3), 399 (2017). DOI 10.1364/OL.42.000399
95. J. Lu, Y. Dai, Q. Li, Y. Zhang, C. Wang, F. Pang, T. Wang, X. Zeng, *Nanoscale* **11**, 908 (2019). DOI 10.1039/C8NR06078A
96. A. Ròdenas, M. Gu, G. Corrielli, P. Paiè, S. John, A.K. Kar, R. Osellame, *Nat. Photonics* **13**(2), 105 (2019). DOI 10.1038/s41566-018-0327-9
97. E. Yablonovitch, *Phys. Rev. Lett.* **58**, 2059 (1987). DOI 10.1103/PhysRevLett.58.2059
98. S. John, *Phys. Rev. Lett.* **58**, 2486 (1987). DOI 10.1103/PhysRevLett.58.2486
99. G. Cheng, C. D'Amico, X. Liu, R. Stoian, *Opt. Lett.* **38**(11), 1924 (2013). DOI 10.1364/OL.38.001924
100. F. Sima, K. Sugioka, *Nanophotonics* **10**(9), 2389 (2021). DOI 10.1515/nanoph-2021-0159
101. M. Bellec, L. Canioni, A. Royon, B. Bousquet, J. Degert, E. Freysz, T. Cardinal, J.F. Letard, in *Data Storage*, ed. by F. Balasa (InTech, 2010), pp. 33–51. DOI 10.5772/8874
102. J. Zhang, M. Gecevičius, M. Beresna, P.G. Kazansky, *Phys. Rev. Lett.* **112**, 033901 (2014). DOI 10.1103/PhysRevLett.112.033901
103. Y. Liu, G. Chen, M. Song, X. Ci, B. Wu, E. Wu, H. Zeng, *Opt. Express* **21**(10), 12843 (2013). DOI 10.1364/OE.21.012843
104. V.V. Kononenko, I.I. Vlasov, V.M. Gololobov, T.V. Kononenko, T.A. Semenov, A.A. Khomich, V.A. Shershulin, V.S. Krivobok, V.I. Konov, *Appl. Phys. Lett.* **111**(8), 081101 (2017). DOI 10.1063/1.4993751
105. Y.C. Chen, P.S. Salter, S. Knauer, L. Weng, A.C. Frangeskou, C.J. Stephen, S.N. Ishmael, P.R. Dolan, S. Johnson, B.L. Green, G.W. Morley, M.E. Newton, J.G. Rarity, M.J. Booth, J.M. Smith, *Nat. Photonics* **11**(2), 77 (2017). DOI 10.1038/nphoton.2016.234
106. J.P. Hadden, V. Bharadwaj, B. Sotillo, S. Rampini, R. Osellame, J.D. Witmer, H. Jayakumar, T.T. Fernandez, A. Chiappini, C. Armellini, M. Ferrari, R. Ramponi, P.E. Barclay, S.M. Eaton, *Opt. Lett.* **43**(15), 3586 (2018). DOI 10.1364/OL.43.003586
107. A.G.J. MacFarlane, J.P. Dowling, G.J. Milburn, *Philosophical Transactions of the Royal Society of London. Series A: Mathematical, Physical and Engineering Sciences* **361**(1809), 1655 (2003). DOI 10.1098/rsta.2003.1227
108. N. Gisin, R. Thew, *Nat. Photonics* **1**(3), 165 (2007). DOI 10.1038/nphoton.2007.22
109. T. Meany, M. Gräfe, R. Heilmann, A. Perez-Leija, S. Gross, M.J. Steel, M.J. Withford, A. Szameit, *Laser Photonics Rev.* **9**(4), 363 (2015). DOI 10.1002/lpor.201500061
110. A.W. Schell, J. Kaschke, J. Fischer, R. Henze, J. Wolters, M. Wegener, O. Benson, *Sci. Rep.* **3**, 1577 (2013). DOI 10.1038/srep01577
111. G. Corrielli, A. Crespi, R. Osellame, *Nanophotonics* **10**(15), 3789 (2021). DOI doi:10.1515/nanoph-2021-0419
112. Microsoft silica project. URL <https://www.microsoft.com/en-us/research/project/project-silica/>
113. K.O. Hill, Y. Fujii, D.C. Johnson, B.S. Kawasaki, *Appl. Phys. Lett.* **32**(10), 647 (1978). DOI 10.1063/1.89881
114. A. Cusano, A. Cutolo, J. Albert, *Fiber Bragg Grating Sensors: Recent Advancements, Industrial Applications and Market Exploitation* (Bentham Science Publishers, 2011). DOI 10.2174/97816080508401110101
115. S.J. Mihailov, C.W. Smelser, P. Lu, R.B. Walker, D. Grobnic, H. Ding, G. Henderson, J. Unruh, *Opt. Lett.* **28**(12), 995 (2003). DOI 10.1364/OL.28.000995
116. J. Thomas, E. Wikszak, T. Clausnitzer, U. Fuchs, U. Zeitner, S. Nolte, A. Tünnermann, *Appl. Phys. A* **86**(2), 153 (2007). DOI 10.1007/s00339-006-3754-2
117. A. Martinez, M. Dubov, I. Khrushchev, I. Bennion, *Electron. Lett.* **40**, 1170 (2004)
118. M. Ams, P. Dekker, S. Gross, M.J. Withford, *Nanophotonics* **6**(5), 743 (2017). DOI doi:10.1515/nanoph-2016-0119

119. G.D. Marshall, M. Ams, M.J. Withford, *Opt. Lett.* **31**(18), 2690 (2006). DOI 10.1364/OL.31.002690
120. M. Thiel, G. Flachenecker, W. Schade, *Opt. Lett.* **40**(7), 1266 (2015). DOI 10.1364/OL.40.001266
121. Y. Cheng, K. Sugioka, K. Midorikawa, M. Masuda, K. Toyoda, M. Kawachi, K. Shihoyama, *Opt. Lett.* **28**(1), 55 (2003). DOI 10.1364/OL.28.000055
122. G.D. Marshall, A. Jesacher, A. Thayil, M.J. Withford, M. Booth, *Opt. Lett.* **36**(5), 695 (2011). DOI 10.1364/OL.36.000695
123. R.J. Williams, C. Voigtländer, G.D. Marshall, A. Tünnermann, S. Nolte, M.J. Steel, M.J. Withford, *Opt. Lett.* **36**(15), 2988 (2011). DOI 10.1364/OL.36.002988
124. H. Zhang, P.R. Herman, in *Bragg Gratings, Photosensitivity, and Poling in Glass Waveguides* (Optical Society of America, 2007), p. BTuD4. DOI 10.1364/BGPP.2007.BTuD4
125. H. Zhang, P.R. Herman, *IEEE Photon. Technol. Lett.* **21**(5), 277 (2009). DOI 10.1109/LPT.2008.2010717
126. M. Ams, P. Dekker, G.D. Marshall, M.J. Withford, *Opt. Lett.* **37**(6), 993 (2012). DOI 10.1364/OL.37.000993
127. E. Ertorer, M. Haque, J. Li, P.R. Herman, *Opt. Express* **26**(7), 9323 (2018). DOI 10.1364/OE.26.009323
128. G. Zhang, G. Cheng, M.K. Bhuyan, C. D'Amico, Y. Wang, R. Stoian, *Photon. Res.* **7**(7), 806 (2019). DOI 10.1364/PRJ.7.000806
129. G. Zhang, G. Cheng, M. Bhuyan, C. D'Amico, R. Stoian, *Opt. Lett.* **43**(9), 2161 (2018). DOI 10.1364/OL.43.002161
130. R. Kashyap, in *Fiber Bragg Gratings (Second Edition)*, ed. by R. Kashyap (Academic Press, Boston, 2010), pp. xvii–xviii. DOI 10.1016/B978-0-12-372579-0.00019-3
131. H. Zhang, S. Ho, S.M. Eaton, J. Li, P.R. Herman, *Opt. Express* **16**(18), 14015 (2008). DOI 10.1364/OE.16.014015
132. K.K. Lee, A. Mariampillai, M. Haque, B.A. Standish, V.X. Yang, P.R. Herman, *Opt. Express* **21**(20), 24076 (2013). DOI 10.1364/OE.21.024076
133. I. Spaleniak, S. Gross, N. Jovanovic, R.J. Williams, J.S. Lawrence, M.J. Ireland, M.J. Withford, *Laser Photonics Rev.* **8**(1), L1 (2014). DOI 10.1002/lpor.201300129
134. J. Bland-Hawthorn, M. Englund, G. Edvell, *Opt. Express* **12**(24), 5902 (2004). DOI 10.1364/OPEX.12.005902
135. G.D. Marshall, P. Dekker, M. Ams, J.A. Piper, M.J. Withford, *Opt. Lett.* **33**(9), 956 (2008). DOI 10.1364/OL.33.000956
136. J.R. Grenier, L.A. Fernandes, P.R. Herman, *Opt. Express* **21**(4), 4493 (2013). DOI 10.1364/OE.21.004493
137. V. Maselli, J.R. Grenier, S. Ho, P.R. Herman, *Opt. Express* **17**(14), 11719 (2009). DOI 10.1364/OE.17.011719
138. E. Le Coarer, S. Blaize, P. Benech, I. Stefanon, A. Morand, G. Léron del, G. Leblond, P. Kern, J.M. Fedeli, P. Royer, *Nat. Photonics* **1**(8), 473 (2007). DOI 10.1038/nphoton.2007.138
139. M. Bonduelle, G. Martin, I.H. Perez, A. Morand, C. D'Amico, R. Stoian, G. Zhang, G. Cheng, in *Optical and Infrared Interferometry and Imaging VII*, vol. 11446 (SPIE, 2020), vol. 11446, pp. 621–633. DOI 10.1117/12.2562179
140. C. D'Amico, G. Martin, J. Troles, G. Cheng, R. Stoian, *Photonics* **8**(6), 211 (2021). DOI 10.3390/photonics8060211
141. G. Martin, M. Bhuyan, J. Troles, C. D'Amico, R. Stoian, E.L. Coarer, *Opt. Express* **25**(7), 8386 (2017). DOI 10.1364/OE.25.008386
142. T.A. Birks, I. Gris-Sánchez, S. Yerolatsitis, S.G. Leon-Saval, R.R. Thomson, *Adv. Opt. Photon.* **7**(2), 107 (2015). DOI 10.1364/AOP.7.000107
143. R.R. Thomson, A.K. Kar, J. Allington-Smith, *Opt. Express* **17**(3), 1963 (2009). DOI 10.1364/OE.17.001963
144. J.J. Bryant, R.R. Thomson, M.J. Withford, *Opt. Express* **25**(17), 19966 (2017). DOI 10.1364/OE.25.019966
145. S. Minardi, R.J. Harris, L. Labadie, *Astron. Astrophys. Rev.* **29**(1), 6 (2021). DOI 10.1007/s00159-021-00134-7

146. Y. Kondo, J. Qiu, T. Mitsuyu, K. Hirao, T. Yoko, *Jpn. J. Appl. Phys.* **38**(10A), L1146 (1999). DOI 10.1143/JJAP.38.L1146
147. A. Marcinkevičius, S. Juodkazis, M. Watanabe, M. Miwa, S. Matsuo, H. Misawa, J. Nishii, *Opt. Lett.* **26**(5), 277 (2001). DOI 10.1364/OL.26.000277
148. Y. Bellouard, A. Said, M. Dugan, P. Bado, *Opt. Express* **12**(10), 2120 (2004). DOI 10.1364/OPEX.12.002120
149. P. Vlugter, E. Block, Y. Bellouard, *Phys. Rev. Materials* **3**, 053802 (2019). DOI 10.1103/PhysRevMaterials.3.053802
150. Y. Bellouard, *Opt. Express* **23**(22), 29258 (2015). DOI 10.1364/OE.23.029258
151. Y. Bellouard, A. Champion, B. McMillen, S. Mukherjee, R.R. Thomson, C. Pépin, P. Gillet, Y. Cheng, *Optica* **3**(12), 1285 (2016). DOI 10.1364/OPTICA.3.001285
152. Y. Bellouard, M. Dugan, A.A. Said, P. Bado, *Appl. Phys. Lett.* **89**(16), 161911 (2006). DOI 10.1063/1.2363957
153. J. Morikawa, E. Hayakawa, T. Hashimoto, R. Buividas, S. Juodkazis, *Opt. Express* **19**(21), 20542 (2011). DOI 10.1364/OE.19.020542
154. Y. Bellouard, T. Colomb, C. Depeursinge, M. Dugan, A.A. Said, P. Bado, *Opt. Express* **14**(18), 8360 (2006). DOI 10.1364/OE.14.008360
155. P. Vlugter, Y. Bellouard, *Phys. Rev. Materials* **4**, 023607 (2020). DOI 10.1103/PhysRevMaterials.4.023607
156. R. Lacroix, V. Chomienne, G. Kermouche, J. Teisseire, E. Barthel, S. Queste, *Int. J. Appl. Glass Sci.* **3**(1), 36 (2012). DOI <https://doi.org/10.1111/j.2041-1294.2011.00075.x>
157. A. Champion, Y. Bellouard, *Opt. Mater. Express* **2**(6), 789 (2012). DOI 10.1364/OME.2.000789
158. P. Vlugter, Y. Bellouard, *Phys. Rev. Materials* **6**, 033602 (2022). DOI 10.1103/PhysRevMaterials.6.033602
159. T. Zhang, C. Godavarthi, P.C. Chaumet, G. Maire, H. Giovannini, A. Talneau, M. Allain, K. Belkebir, A. Sentenac, *Optica* **3**(6), 609 (2016). DOI 10.1364/OPTICA.3.000609